CHAPTER FIVE

Planar Kinematic Modeling and Analysis

The mathematical and numerical aspects of kinematic analysis were stressed in Chapters 3 and 4. Examples involving even very simple systems have shown that the nonlinear character of the equations of kinematics leads to potential analytical, computational, and practical performance difficulties. The objective of this chapter is to present and illustrate the use of modeling and analysis concepts that exploit and reinforce physical intuition. A judicious combination of complementary physical and mathematical reasoning can be invaluable in the kinematic analysis of realistic mechanical systems. This is especially the case when a computer code such as DADS is employed for automated formulation and solution of kinematic equations. The availability of such computer codes encourages engineers to analyze actual systems, with large-scale realistic models. Effective utilization of such a resource, however, requires that the engineer create models that represent reality, recognize and correct modeling errors, recognize infeasible or marginal designs, and use analysis tools to create and test improved designs. Happily, many of the intuitive aids that are used in conventional design analysis are also valuable in computer-aided analysis and design.

A general approach to the art of kinematic modeling and analysis is suggested in Section 5.1. Analyses of specific systems, with the aid of the DADS code [27], are presented in the remaining sections of the chapter. As in most arts, learning to use kinematic analysis tools is enhanced by practice. Project-oriented problems are given at the end of the chapter. Readers are encouraged to try the methods presented and illustrated in this chapter on these problems or, even better, on applications of their own choosing.

5.1 MODELING AND ANALYSIS TECHNIQUES

Kinematic modeling of a mechanism involves the selection of bodies that make up the mechanism, kinematic constraints that act between pairs of bodies, and

time-dependent kinematic drivers. A key requirement of kinematic modeling is that the combination of bodies, kinematic constraints, and drivers must have no free degrees of freedom. That is, the number of generalized coordinates in the model must equal the number of independent constraint equations. Since composite joints define constraints that are imposed by coupler components, without introducing generalized coordinates for the coupler, they reduce the number of computations required to solve position, velocity, and acceleration equations.

Once the bodies that make up a system model have been selected, a body-fixed reference frame must be attached to each body. Since kinematic analysis is not concerned with forces and inertias, the locations of the origins of body-fixed reference frames are arbitrary. They can be located at points that make the model easy to develop. If subsequent dynamic analysis is anticipated, however, body-fixed reference frames with their origins at centers of mass should be selected (see Chapter 6).

A careful sketch of each body should be made and used to define data for analysis. The old adage "a picture is worth a thousand words" is as true in kinematic modeling as it is in the art of communication.

In addition to specifying joints, an initial estimate of the position and orientation of each body must be provided in order to assemble the system. Estimates of x, y, and ϕ for each body can be obtained from a reasonably scaled diagram of the system. While estimates should be reasonably accurate, extreme precision is not required, since the assembly mode of analysis uses an optimization algorithm to assemble the system.

After specification of bodies and kinematic constraints, one or more degrees of freedom will remain. To complete the model, a number of drivers equal to the number of degrees of freedom must be specified. Drivers usually define relative or absolute motion that is imposed by actuators or by specifying some characteristics of the motion that is desired, regardless of the prime mover that is used to generate the motion.

Upon completion of kinematic analysis, the positions, velocities, and accelerations of each body are available at each time step in the time interval under consideration. This can be a "curse of riches," since the quantity of output data can be overwhelming, making analysis of the data difficult. The use of a postprocessor to tabulate, graph, or animate data is especially valuable.

While automated computational checks are carried out in the DADS code to warn the user that an infeasible design or redundant constraints may have been specified, it is good engineering practice to formulate a reasonable model of the system that is intended. The process of kinematic modeling is partially an engineering art that requires physical insight and intuition. To assist the engineer in modeling, the following *kinematic modeling recipe* is suggested, making use of theoretical information and intuition to arrive at a reasonable model:

1. Draw a clear diagram of the system to be modeled and select and name

or number bodies and kinematic joints between pairs of bodies. As preliminary checks on reasonableness of the model:

a. Count the number nh of constraint equations that have been defined and calculate $d = 3nb - nh$, where nb is the number of bodies in the model. If the constraints specified are independent, d is the number of degrees of freedom of the system. Since the engineer generally knows how many degrees of freedom are intended, this is a good check on the reasonableness of the model. If $d \leq 0$, or if d is less than the number of degrees of freedom anticipated, very likely redundant constraints have been defined. While agreement of d with the number of degrees of freedom intended does not guarantee a good model, it is certainly necessary.

b. Inspect the model for feasibility by asking the question, "If there is any manufacturing imperfection in the model; can the system be assembled?" The foundation for this check is explained in Section 3.7. If the system can be assembled with the data defined, but not with imperfectly fabricated joints, then redundant constraints are present. If it cannot be assembled with even the nominal data, then an infeasible design has been specified.

2. Presuming redundant constraints have been eliminated, define $d = 3nb - nh$ drivers to specify the motion of the system. Repeat the analysis of step 1b to evaluate the feasibility and redundancy of the driving constraints that have been specified.

3. Make drawings of each body in the system, defining the body-fixed x'-y' frames and data required for each of the kinematic joints and drivers selected, according to the formulations presented in Chapter 3. Tabulate the data required to specify bodies and joints.

4. Use a reasonable sketch or diagram of the system to estimate the position and orientation variables to initiate the assembly process of analysis.

While this suggested procedure is not guaranteed to find all flaws in models, it can provide a foundation on which to gain engineering confidence in the model selected. To illustrate the use of the procedure, consider the following elementary example.

Example 5.1.1: The five-bar parallelogram mechanism shown in Fig. 5.1.1, with cross bars of unit length, might be modeled with six revolute joints and three absolute constraints to fix body 5 as ground. To check the reasonableness of this model, first count to see if the single degree of freedom is $1 = 3nb - nh$. Here $nb = 5$ and $nh = 3 + 6 \times 2 = 15$. Thus, $3nb - nh = 15 - 15 = 0 \neq 1$, so something is wrong.

To see what is wrong, note that if ϕ_1 is fixed then ϕ_2 is known and the revolute joint definition point on body 4, for the joint between bodies 3 and 4, is

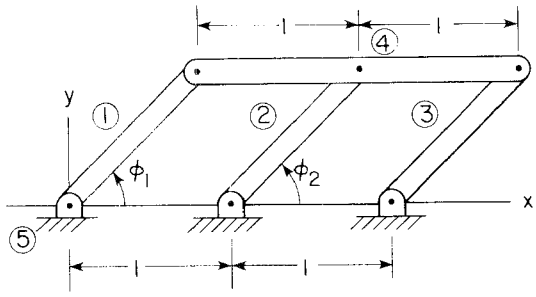

Figure 5.1.1 Five-bar parallelogram mechanism.

fixed in the x-y plane. If the length of bar 3 is slightly greater than 1, it cannot be inserted into the mechanism. Thus, the revolute joint between bars 3 and 4 contains a redundancy. If it is replaced by a revolute–translational joint between bars 3 and 4, then the mechanism can be assembled, as indicated in Fig. 5.1.2. In this model, $nh = 3 + 5 \times 2 + 1 = 14$, so $3nb - nh = 15 - 14 = 1$ and the counting criteria is satisfied.

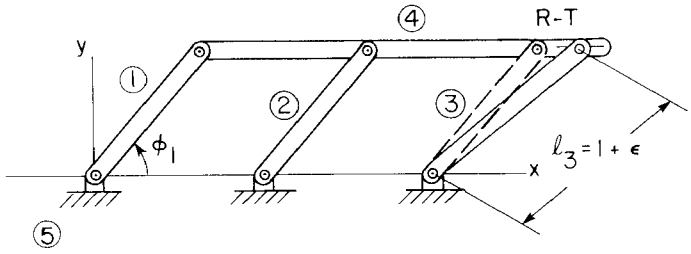

Figure 5.1.2 Five-bar imperfect parallelogram mechanism.

With $\phi_1 = \omega t$ as a driver, as long as $\phi_1 \neq k\pi$, $k = 0, 1, \ldots$, if $\ell_3 > 1$ the mechanism of Fig. 5.1.2 performs well. If $\ell_3 = 1$, however, then a problem is encountered at $\phi_1 = \pi/2$, as seen physically in Fig. 5.1.3. As ϕ_1 passes just beyond $\pi/2$, the slider point on body 3 can move either to the left or to the

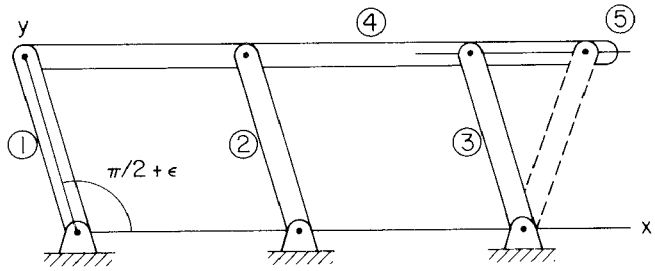

Figure 5.1.3 Bifurcation point for five-bar parallelogram mechanism.

right. Thus, $\phi_1 = \omega t^* = \pi/2$ is a bifurcation point and the constraint Jacobian that contains the driver must be singular. It is interesting that this physical reasoning shows that the 15×15 Jacobian matrix is singular, without evaluating its determinant or calculating its rank using Gaussian elimination. This illustrates the value of complementary physical and mathematical reasoning in kinematic modeling and analysis. Finally, if $\ell_3 < 1$, a lock-up singularity will be encountered prior to t^*.

5.2 KINEMATIC ANALYSIS OF A SLIDER–CRANK MECHANISM

The slider–crank mechanism of Fig. 2.4.6 is one of the most commonly used machine subsystems in mechanical system design. It is employed as the principal element of internal combustion engines (Fig. 1.1.1), compressors, fly-ball governors (Fig. 1.1.3), stamping machines (Fig. 1.1.2), and many other machines. Analytical kinematic analyses of simplified models of slider–cranks have been carried out in Chapters 2 and 3. The purpose of this section is to systematically analyze the kinematic performance of a slider–crank mechanism, illustrate use of models, investigate the effect of design variations on kinematic performance, and identify lock-up or singular configurations that may occur.

Data used in this section and throughout the text are given in SI units (meter, kilogram, seconds) unless noted otherwise. The specific values used are not intended to represent any particular machine element.

5.2.1 Alternative Models

The slider–crank mechanisms can be modeled in many different ways. Two models are developed here to demonstrate the preparation and analysis of the data required for kinematic analysis. In model 1 (see Fig. 5.2.1), each link and ground is modeled as a body. Joints can then be modeled as revolute and translational joints, as follows:

Model 1		
Bodies		
Four bodies		$nc = 12$
Constraints		
Revolute joints:	A	2
	B	2
	C	2
Translational joint:	D	2
Ground constraints		3
		$nh = 11$
Thus, DOF = 12 − 11 = 1.		

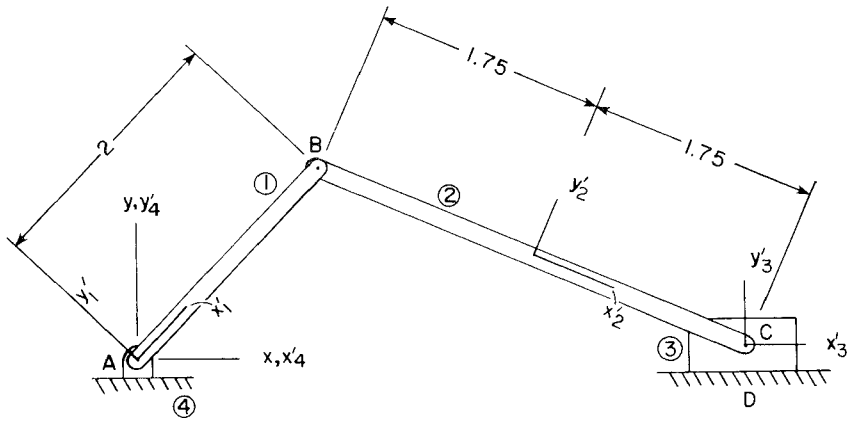

Figure 5.2.1 Slider–crank, model 1.

To eliminate the one remaining DOF, a driver must be introduced. Typically, this would be an angle driver on ϕ_1.

To define each revolute joint, the common point P between bodies connected must be defined in the body-fixed frame. The three revolute joints in model 1 are defined in Table 5.2.1.

TABLE 5.2.1 Revolute Joint Data, Model 1

Joint	1	2	3
Common point P	A	B	C
Body i	4	1	2
$x_i'^P$	0.0	2.0	1.75
$y_i'^P$	0.0	0.0	0.0
Body j	1	2	3
$x_j'^P$	0.0	−1.75	0.0
$y_j'^P$	0.0	0.0	0.0

To define a translational joint, two parallel vectors, one on each body connected, must be defined. Vectors $\mathbf{v}_4$ and $\mathbf{v}_3$ are fixed in bodies 4 and 3, respectively (see Fig. 5.2.2). Coordinates of the points that define these two vectors, in their respective body-fixed frames, are given in Table 5.2.2.

Figure 5.2.2 Translational joint, model 1.

TABLE 5.2.2 Translational Joint Data, Model 1

Vector	$\mathbf{v}_4$	$\mathbf{v}_3$
$x_i'^P$	$x_4'^P = 0.0$	$x_3'^P = 0.0$
$y_i'^P$	$y_4'^P = 0.0$	$y_3'^P = 0.0$
$x_i'^Q$	$x_4'^Q = 1.0$	$x_3'^Q = 1.0$
$y_i'^Q$	$y_4'^Q = 0.0$	$y_3'^Q = 0.0$

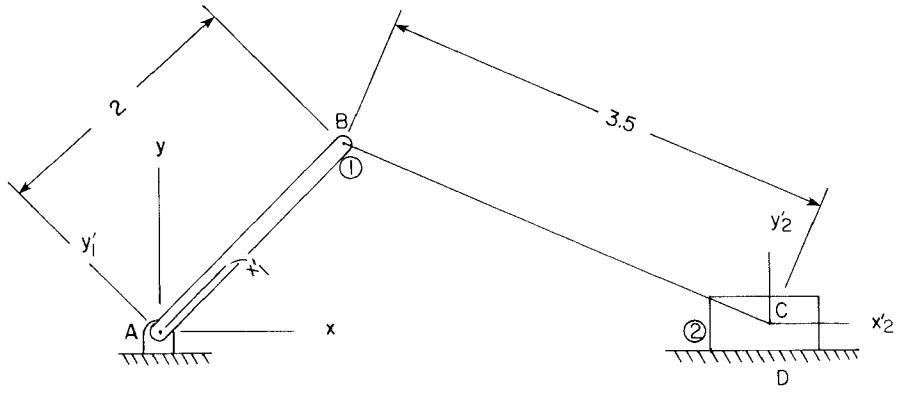

Figure 5.2.3 Slider–crank, model 2.

In model 2 (see Fig. 5.2.3), the connecting rod BC is modeled as a composite revolute–revolute joint and no ground body is introduced. The advantage of the composite joint is that it reduces the dimension of the matrices that must be handled by eliminating three generalized coordinates that would normally be required for the connecting rod. This mechanism is modeled using absolute constraints to represent the rotational joint at point A and the translational joint at point C, as follows:

Model 2	
Bodies	
Two bodies	$nc = 6$
Constraints	
Body 1 absolute constraints: $x_1 = 0$	1
$y_1 = 0$	1
Body 2 absolute constraints: $y_2 = 0$	1
$\phi_2 = 0$	1
Revolute–revolute joint	1
	$nh = 5$
Thus, DOF = 6 − 5 = 1.	

TABLE 5.2.3 Revolute–Revolute Joint *B–C*, Model 2

Length of $BC = 3.5$	
Point B (body 1)	Point C (body 2)
$x_1'^B = 2.0$	$x_2'^C = 0.0$
$y_1'^B = 0.0$	$y_2'^C = 0.0$

The absolute constraints on body 2 are equivalent to a translational joint, prohibiting rotation and y translation of the body. Similarly, the absolute constraints on body 1 are equivalent to a revolute joint. To specify a revolute–revolute joint, the end points of the coupler on the bodies that are connected must be specified in their respective body-fixed frames, and the length of the link must be provided. Table 5.2.3 contains data for this joint.

5.2.2 Assembly Analysis

For model 1, Fig. 5.2.1 can be used as the source for position and orientation estimates. Assuming a scale of 1:1, the position and angular orientation of each body can be measured. To show the power of the assembly technique discussed in Section 4.3, the poor initial estimate given in Table 5.2.4 and shown in Fig. 5.2.4 is used.

TABLE 5.2.4 Initial Estimate, Model 1

Body no.	1	2	3	4
x	−0.5	3.0	5.0	0.0
y	0.0	1.0	0.0	0.0
ϕ	0.5	−0.4	0.0	0.0

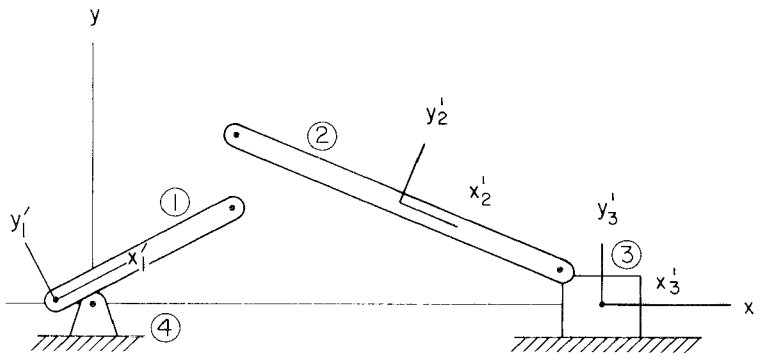

Figure 5.2.4 Initial estimate for slider–crank, model 1.

TABLE 5.2.5 Assembled Configuration without Driver, Model 1

Body no.	1	2	3	4
x	0.0	3.1702	4.992	0.0
y	0.0	0.6387	0.0	0.0
ϕ	0.6916	−0.3728	0.0	0.0

The system is first assembled without consideration of a driver. Since the system has one degree of freedom, the kinematic constraint equations have infinitely many solutions. The optimization algorithm converges to a solution that is near to the initial estimate. The solution found is tabulated in Table 5.2.5 and illustrated as the solid line drawing in Fig. 5.2.5.

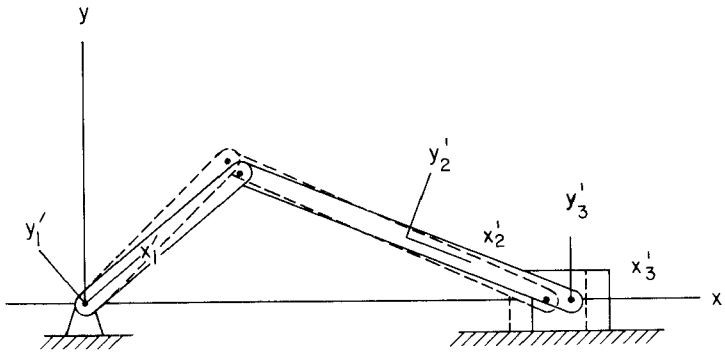

Figure 5.2.5 Assembled slider–crank, model 1.

The next step is to assemble the slider–crank mechanism with the driver $\phi_1 = \pi/4 + \omega t$. The initially ($t = 0$) assembled configuration is tabulated in Table 5.2.6 and illustrated as the dashed line drawing in Fig. 5.2.5.

Consider another initial estimate for which the user made a sign error in estimating the x coordinate of the third body, as shown in Fig. 5.2.6. All other data are the same as in Table 5.2.4. The assembled configuration found by the

TABLE 5.2.6 Assembled Configuration with Driver at $t = 0$, Model 1

Body no.	1	2	3	4
x	0.0	3.0152	4.6162	0.0
y	0.0	0.7066	0.0	0.0
ϕ	0.7852	−0.4158	0.0	0.0

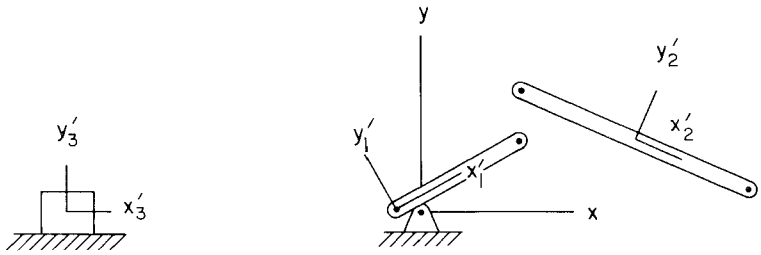

Figure 5.2.6 Erroneous initial estimate, model 1.

optimization algorithm is tabulated in Table 5.2.7 and shown in Fig. 5.2.7 for the same driver. This shows successful assembly of the system, satisfying the driving constraint. However, this is not the configuration that is desired. These variations of initial estimates show that care must be taken to confirm that the assembled configuration is physically meaningful and is the desired configuration.

TABLE 5.2.7 Undesirable Assembled Configuration, Model 1

Body no.	1	2	3	4
x	0.0	−0.1863	−1.7873	0.0
y	0.0	0.7080	0.0	0.0
ϕ	0.7858	−2.7253	0.0	0.0

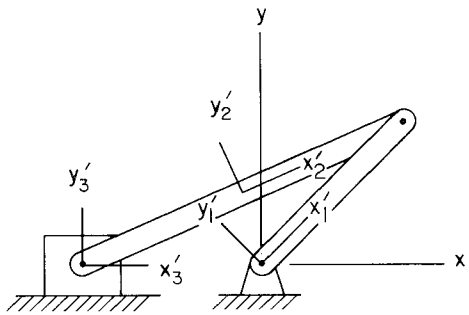

Figure 5.2.7 Undesirable assembled configuration, model 1.

5.2.3 Driver Specification

Since the model has one kinematic degree of freedom, one driver must be specified in order to complete the model. Taking ϕ_1 as the driven coordinate, it

will be specified that body 1 rotates at ω rad/s, with an initial orientation angle of $\phi_1(0) = \pi/4$ rad. The driver is thus specified by the condition

$$\phi_1 = \frac{\pi}{4} + \omega t$$

where ω is the constant angular velocity of the crank (body 1).

5.2.4 Analysis

Kinematic analysis of the slider–crank mechanism, using model 1 with the dimensions of Fig. 5.2.4, is carried out using the DADS code [27]. Two constant driving angular velocities, $\omega_1 = 2\pi$ rad/s and $\omega_2 = 4\pi$ rad/s, are considered (i.e., one and two revolutions per second respectively). Since the motion of the slider (body 3) is of greatest concern in applications, the position (x), velocity ($\dot{x}$), and acceleration ($\ddot{x}$) of the slider are plotted in Figs. 5.2.8, 5.2.9, and 5.2.10, respectively. Identical results are obtained with model 2.

As expected, the mechanism goes through two cycles of motion in one second with ω_2, and the natures of the responses with two driving velocities are

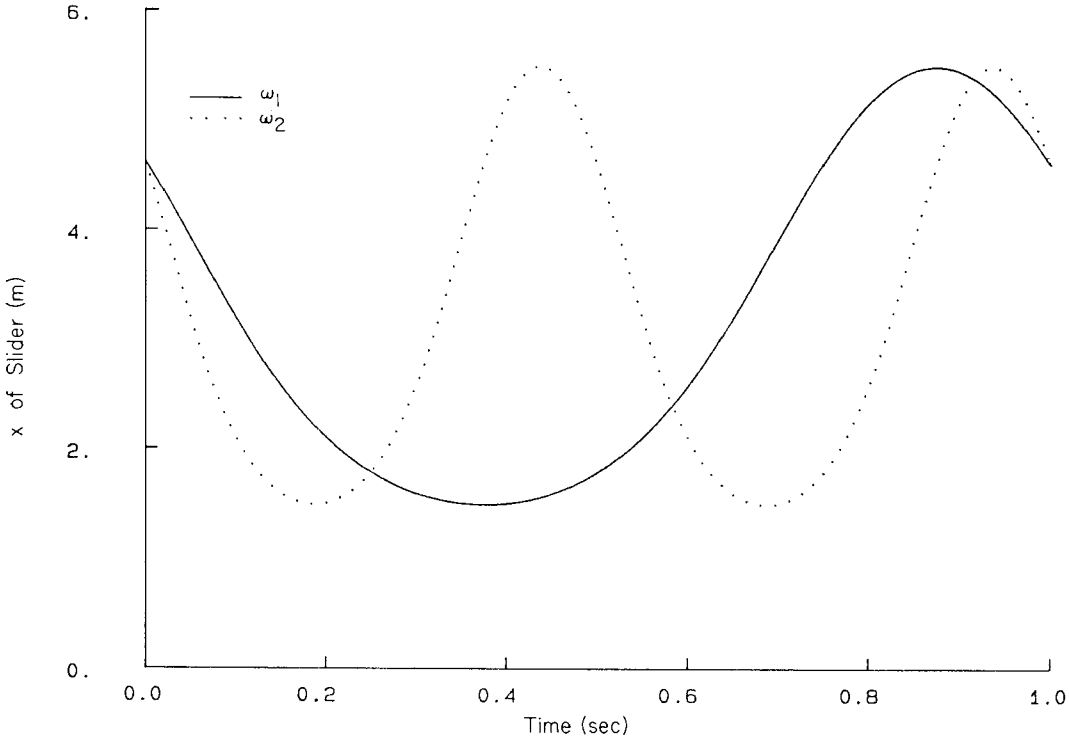

Figure 5.2.8 x of slider versus time, variable ω.

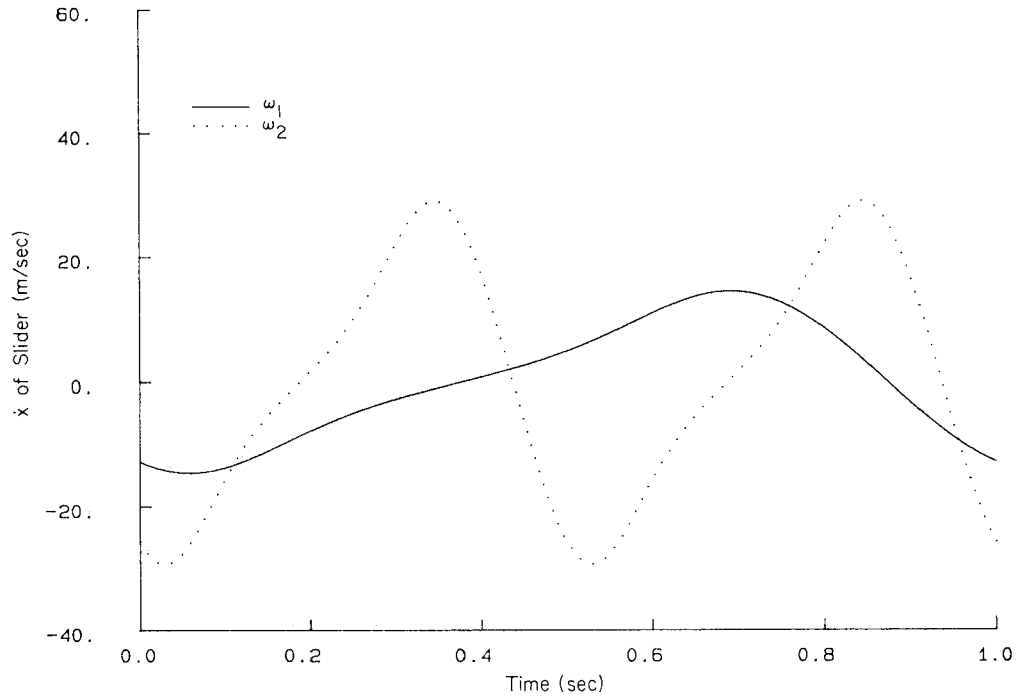

Figure 5.2.9 $\dot{x}$ of slider versus time, variable ω.

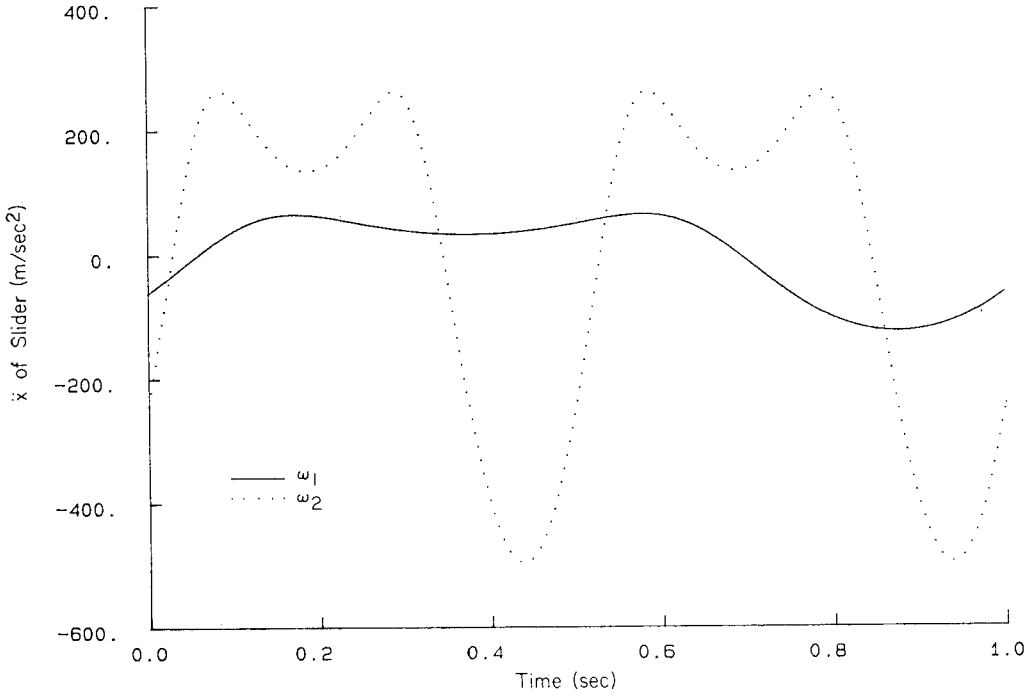

Figure 5.2.10 $\ddot{x}$ of slider versus time, variable ω.

similar. Note, however, that while the stroke lengths are equal for both driving velocities the ratios of maximum velocity and acceleration are approximately 2 and 4, respectively. This suggests that the quadratic terms in velocity on the right side of the acceleration equation are dominating acceleration; that is, these terms grow by a factor of $(2)^2 = 4$ due to the doubled velocity. Since the Jacobian is not changed, acceleration increases by a factor of 4. Thus, increasing operating speed has a much more marked effect on slider acceleration, and hence on bearing loads, than on position and velocity.

To consider the effect of variations in design on the kinematic performance of the slider–crank, let ℓ denote the length of the connecting rod (body 2 in model 1), where $\ell_1 = 3.5$ m is the nominal design considered thus far. Let $\ell_2 = 2.5$, $\ell_3 = 2.2$, and $\ell_4 = 2.1$ be a sequence of decreasing connecting rod lengths. The numerical results of simulations for x, $\dot{x}$, and $\ddot{x}$ of the slider, for each of the four lengths, are shown in Figs. 5.2.11, 5.2.12, and 5.2.13, respectively. Note that position (apart from a translation) and velocity are only moderately sensitive to variation in connecting rod length. Acceleration, on the other hand, shows extreme sensitivity to variation in ℓ, for the smallest values of ℓ, near $t = 0.15$ and 0.6 s. These are times when the slider is near its extreme

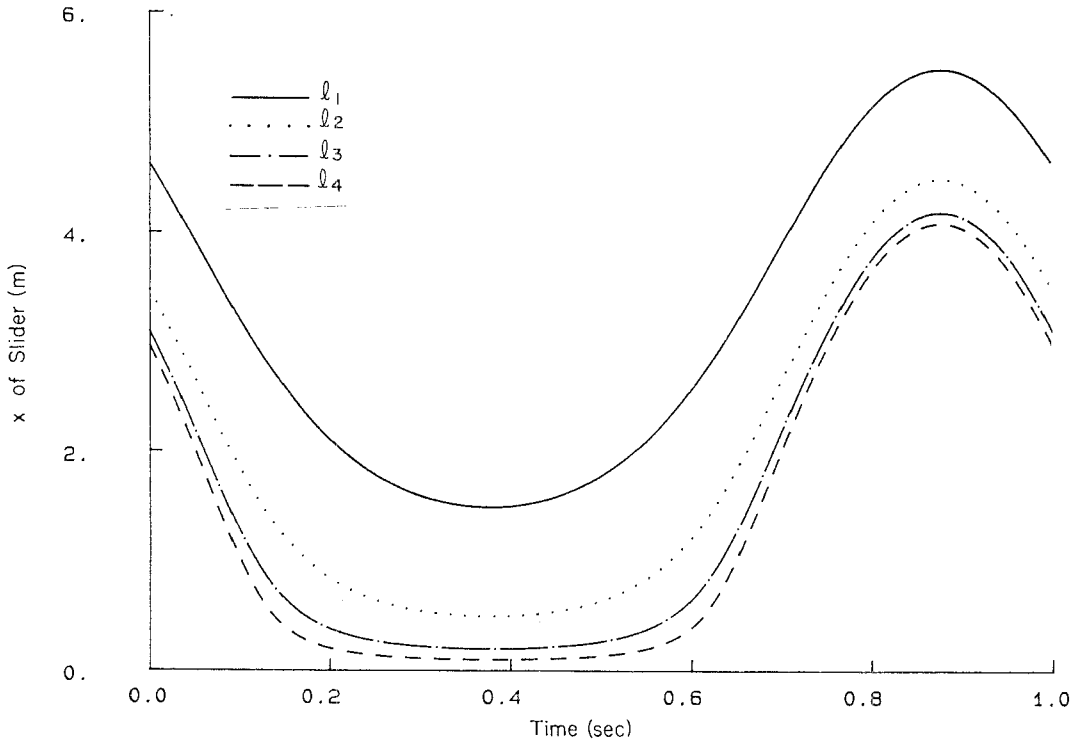

Figure 5.2.11 x of slider versus time, variable ℓ.

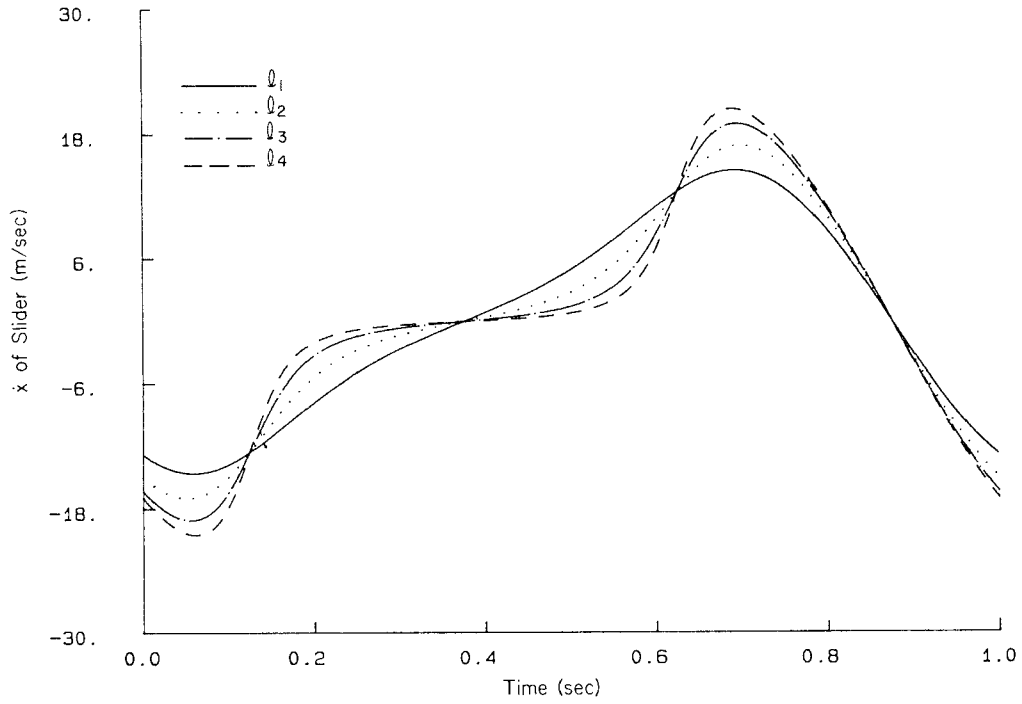

Figure 5.2.12 $\dot{x}$ of slider versus time, variable ℓ.

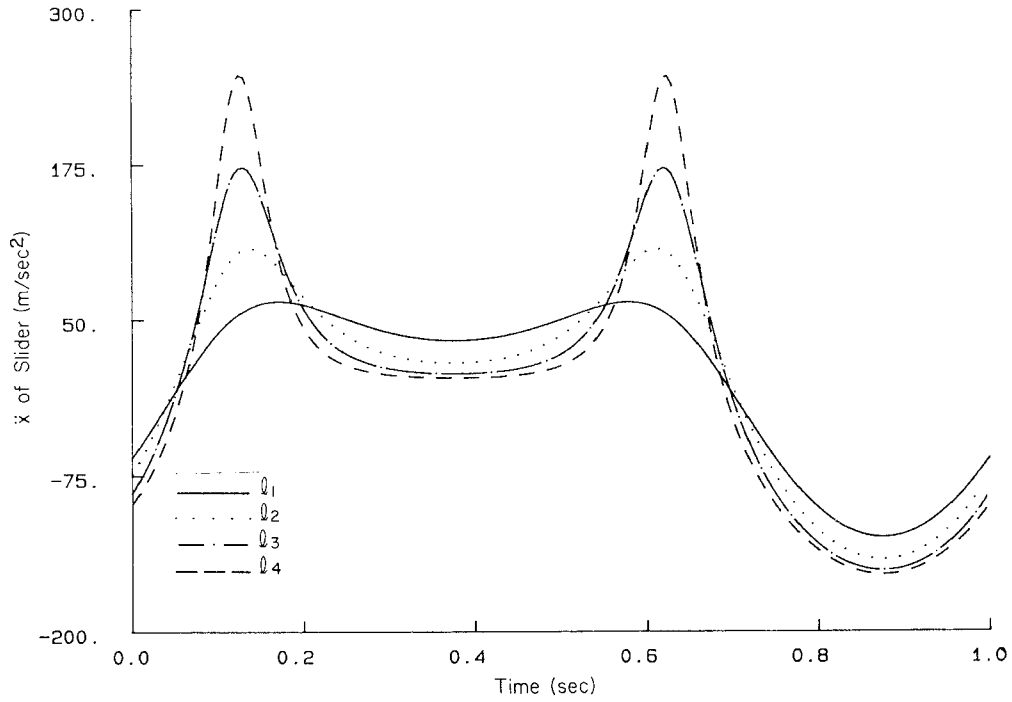

Figure 5.2.13 $\ddot{x}$ of slider versus time, variable ℓ.

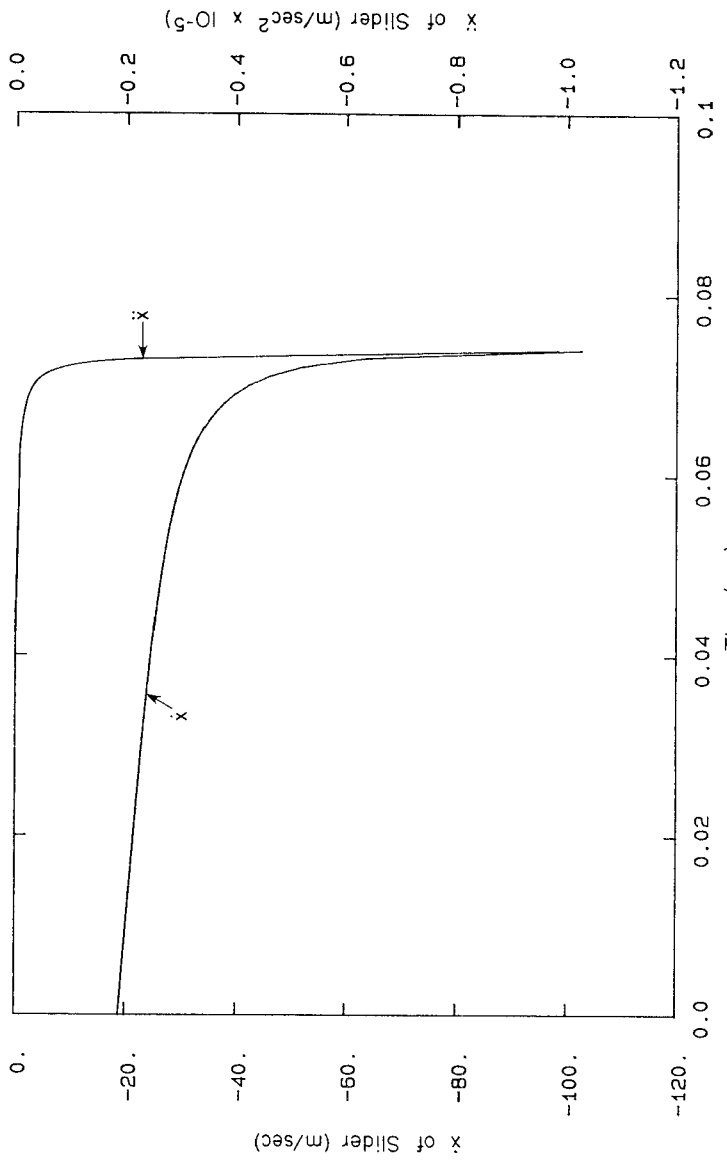

Figure 5.2.14 $\dot{x}$ and $\ddot{x}$ of slider versus time, lock-up case.

right and left positions, respectively. The extreme character of this sensitivity is highlighted by the fact that the peak variation in acceleration between $\ell_3 = 2.2$ and $\ell_4 = 2.1$ is greater than that between $\ell_1 = 3.5$ and $\ell_2 = 2.5$. These results should be expected, based on the singular configuration analysis of Example 3.7.3 and the general guideline that accelerations become very large near singular configurations.

5.2.5 Lock-up Configuration

As shown analytically in Example 3.7.3, the slider–crank mechanism will *lock-up* if the crank arm (body 1) is longer than the connecting rod (body 2). Figure 5.2.14 shows the velocity and acceleration of the slider for a simulation with the length of the slider reduced to $\ell_5 = 1.9$, which is shorter than the length of the crank. Note that as t approaches 0.074 s both the velocity and acceleration of the slider approach infinity. As has been suggested by theoretical considerations in Chapter 3, acceleration shows the more rapid divergence to infinity.

5.3 KINEMATIC ANALYSIS OF A FOUR-BAR MECHANISM

One of the most commonly encountered of the basic mechanisms is the four-bar mechanism shown schematically in Fig. 5.3.1. Examples of the use of this

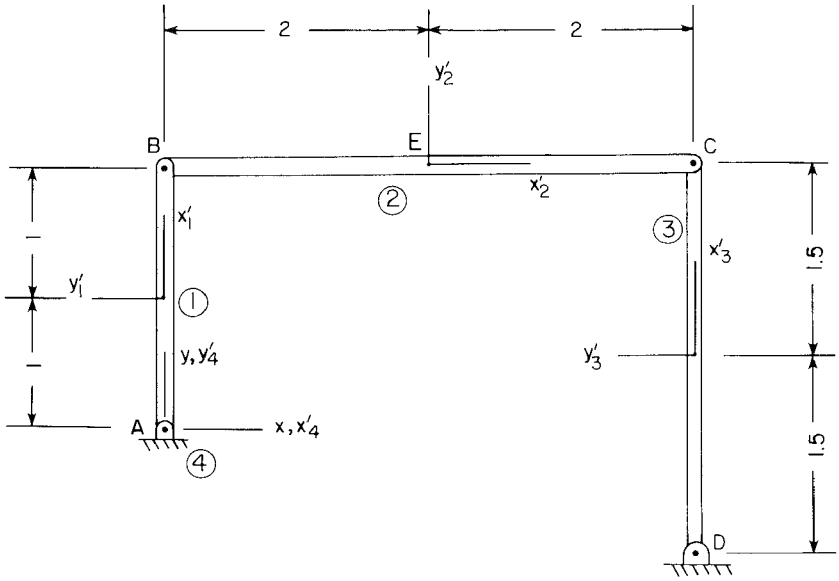

Figure 5.3.1 Four-bar linkage, model 1.

mechanism are the vehicle suspension subsystem (Fig. 1.1.4), windshield wiper (Fig. 1.1.5), and material-handling linkage (Fig. 1.1.6). In some applications, the motion of the coupler (body 2 in Fig. 5.3.1) is controlled by the input angle history of the crank (body 1 in Fig. 5.3.1). In other applications, it is the rotation of the follower (body 3 in Fig. 5.3.1).

5.3.1 Alternative Models

A four-bar mechanism with four revolute joints is modeled here in two different ways. In model 1 (Fig. 5.3.1), each link and ground is modeled as a body.

Four revolute joints complete the model, as follows:

Model 1	
Bodies	
Four bodies	$nc = 12$
Constraints	
Revolute joints: A	2
B	2
C	2
D	2
Ground constraints	3
	$nh = 11$
Thus, DOF = 12 − 11 = 1.	

Revolute joint definition data for this model are given in Table 5.3.1.

TABLE 5.3.1 Revolute Joint Data, Model 1

Joint no.	1	2	3	4
Common point P	A	B	C	D
Body i	4	1	2	3
$x_i'^P$	0.0	1.0	2.0	−1.5
$y_i'^P$	0.0	0.0	0.0	0.0
Body j	1	2	3	4
$x_j'^P$	−1.0	−2.0	1.5	4.0
$y_j'^P$	0.0	0.0	0.0	−1.0

In model 2 (Fig. 5.3.2), link CD is modeled as a revolute–revolute composite joint. Also, the body-fixed frames have been relocated. The mechan-

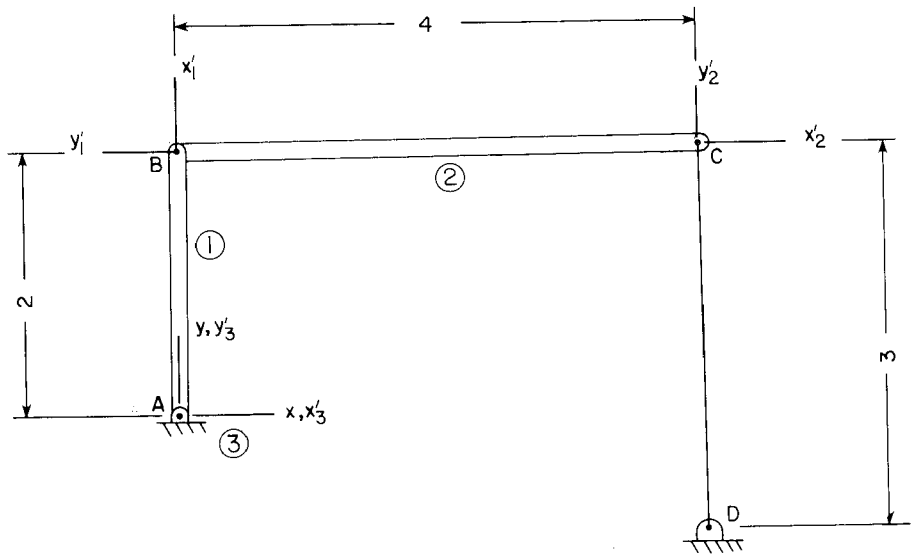

Figure 5.3.2 Four-bar linkage, model 2.

ism can be modeled as follows:

Model 2		
Bodies		
Three bodies		$nc = 9$
Constraints		
Revolute joint:	A	2
	B	2
Revolute–revolute	CD	1
Ground constraints		3
		$nh = 8$
Thus, DOF = 9 − 8 = 1.		

Revolute joint data for model 2 are shown in Table 5.3.2. Table 5.3.3 contains data for the revolute–revolute composite joint.

TABLE 5.3.2 Revolute Joint Data, Model 2

Joint no.	1	2
Common point P	A	B
Body i	3	1
$x_i'^P$	0.0	0.0
$y_i'^P$	0.0	0.0
Body j	1	2
$x_j'^P$	−2.0	−4.0
$y_j'^P$	0.0	0.0

TABLE 5.3.3 Revolute–Revolute Joint Data, Model 2

Length of $CD = 3.0$	
Point C (body 2)	Point D (body 3)
$x_2'^C = 0.0$	$x_3'^D = 4.0$
$y_2'^C = 0.0$	$y_3'^D = -1.0$

5.3.2 Assembly

For model 1, initial position estimates can be measured from Fig. 5.3.1. An intentionally poor initial estimate is tabulated in Table 5.3.4 and shown in Fig. 5.3.3.

TABLE 5.3.4 Initial Estimate, Model 1

Body no.	1	2	3	4
x	0.5	2.1	4.2	0.0
y	0.5	1.9	0.0	0.0
ϕ	1.3	0.1	1.4	0.0

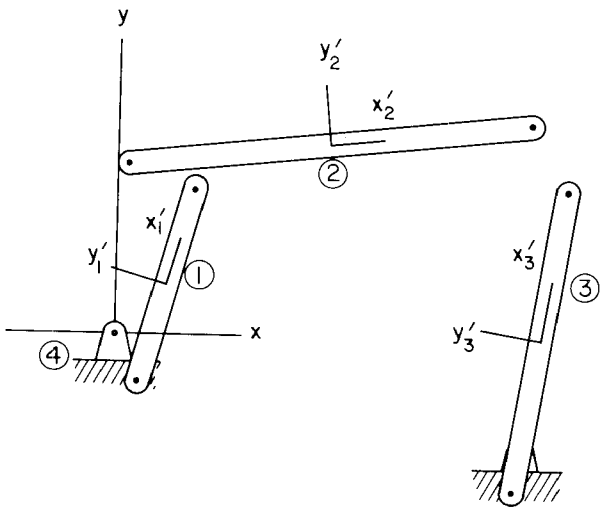

Figure 5.3.3 Initial estimate for four-bar linkage, model 1.

The assembled configuration is tabulated in Table 5.3.5 and shown as a solid line drawing in Fig. 5.3.4. The configuration shown as a dashed line drawing in Fig. 5.3.4 is the assembled configuration at $t = 0$, with the driving constraint $\phi_1 = \pi/2 + 2\pi t$. Numerical values are tabulated in Table 5.3.6.

TABLE 5.3.5 Assembled Configuration without Driver, Model 1

Body no.	1	2	3	4
x	0.2009	2.4002	4.2001	0.0
y	0.9798	1.9664	0.4866	0.0
ϕ	1.3693	0.0034	1.4370	0.0

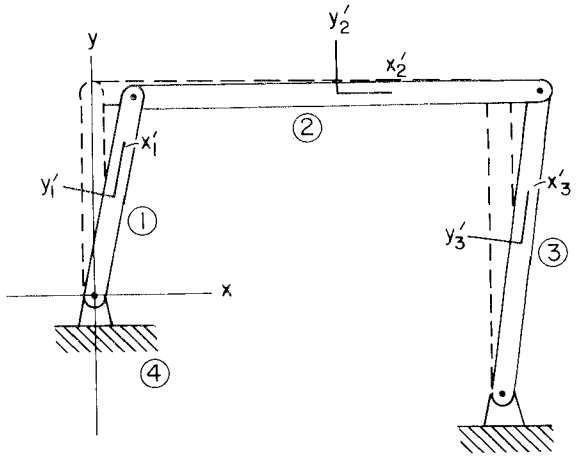

Figure 5.3.4 Assembled four-bar linkage, model 1.

TABLE 5.3.6 Assembled Configuration with Driver, Model 1

Body no.	1	2	3	4
x	0.0	2.0	4.0	0.0
y	1.0	2.0	0.5	0.0
ϕ	1.5708	0.0	1.5708	0.0

5.3.3 Driver Specification

Since the model has only one degree of freedom, one driver must be specified. Taking ϕ_1 as the driven coordinate, it may be driven at 2π rad/s. The driver is specified by

$$\phi_1 = \frac{\pi}{2} + 2\pi t$$

5.3.4 Analysis

Three aspects of the kinematic performance of the mechanism are considered; (1) the path in the x-y plane that is swept out by point E on body 2 (see Fig. 5.3.1), (2) the relation between the follower angle (ϕ_3) and the input angle (ϕ_1), and (3) the follower angular velocity and acceleration as functions of time. To gain insights into these relations as the geometry of the mechanism is changed, consider four lengths of the follower (body 3 in model 1); $\ell_1 = 3$, $\ell_2 = 2.5$, $\ell_3 = 2.2$, and $\ell_4 = 2.1$. As the length of the follower is changed, the y coordinate

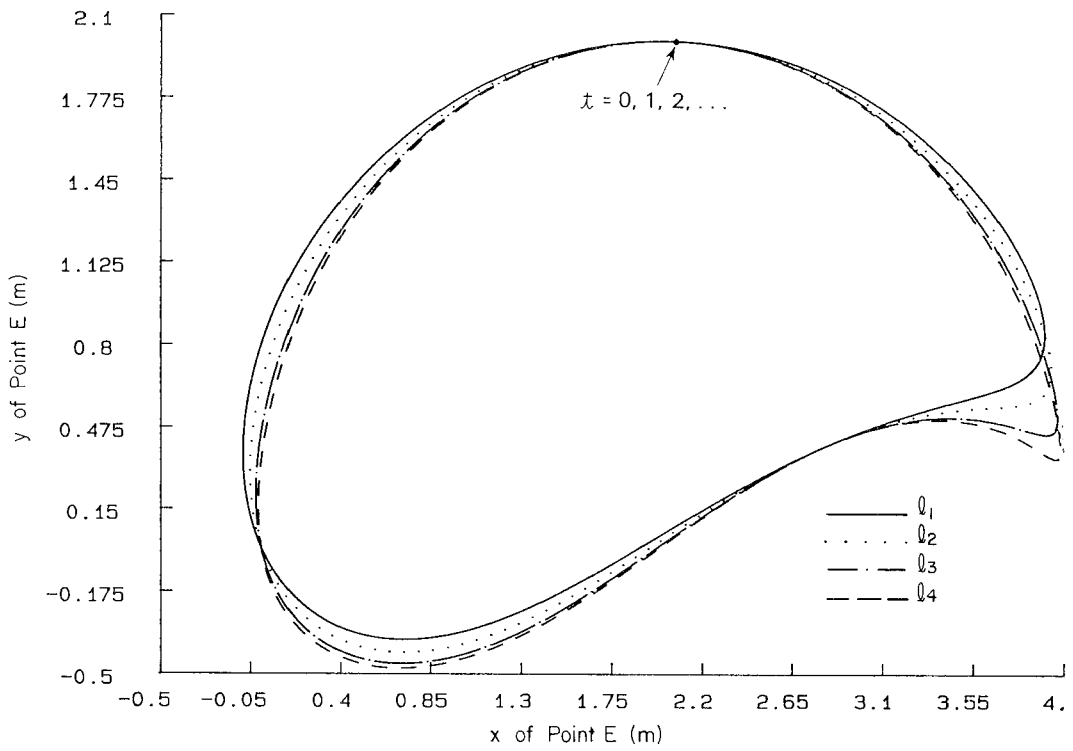

Figure 5.3.5 y versus x coordinates of point E, model 1.

of point D in Fig. 5.3.1 is changed so that when $\phi_1 = \phi_3 = \pi/2$ (as shown in Fig. 5.3.1), $\phi_2 = 0$; that is, the y coordinate of point D is moved upward by the amount the length of body 3 is reduced.

Plots of the y coordinate of point E versus its x coordinate, for each length of body 3, are presented in Fig. 5.3.5. Note that all four of the trajectories have points in common at $t = 0, 1, 2, \ldots$. Note also that, as the length of the follower approaches $\ell = 2$, extreme curvature of the path of point E occurs near the point of the trajectory when E is to the far right. This suggests that some form of singular behavior is impending as the mechanism approaches a parallelogram. This is consistent with the singular behavior noted in Example 3.7.2.

Next, the follower angle (ϕ_3) is plotted versus the crank angle (ϕ_1) for each length of body 3 in Fig. 5.3.6. The extreme variation of ϕ_3 versus ϕ_1 near $\phi_1 = 6.5$ rad is associated with the high curvature noted in Fig. 5.3.5 as ℓ approaches 2.

Finally, plots of the follower angular velocity and angular acceleration as functions of time are presented in Figs. 5.3.7 and 5.3.8 for each length of the follower. The follower angle versus time is not plotted, since it is proportional to

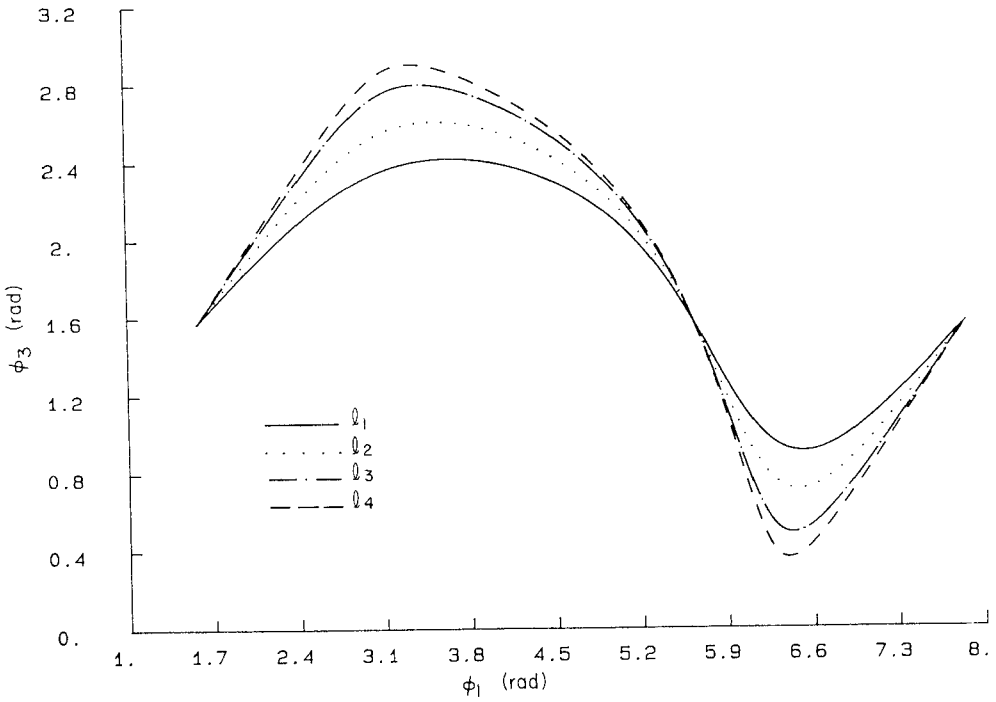

Figure 5.3.6 ϕ of body 3 versus ϕ of body 1, model 1.

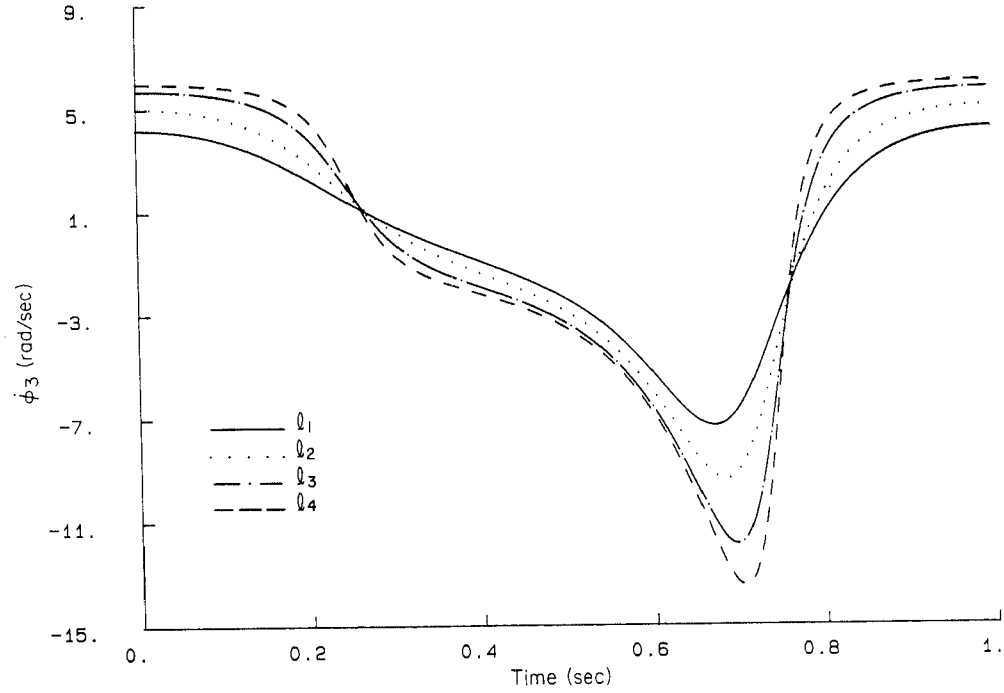

Figure 5.3.7 x of body 1 versus time, model 1.

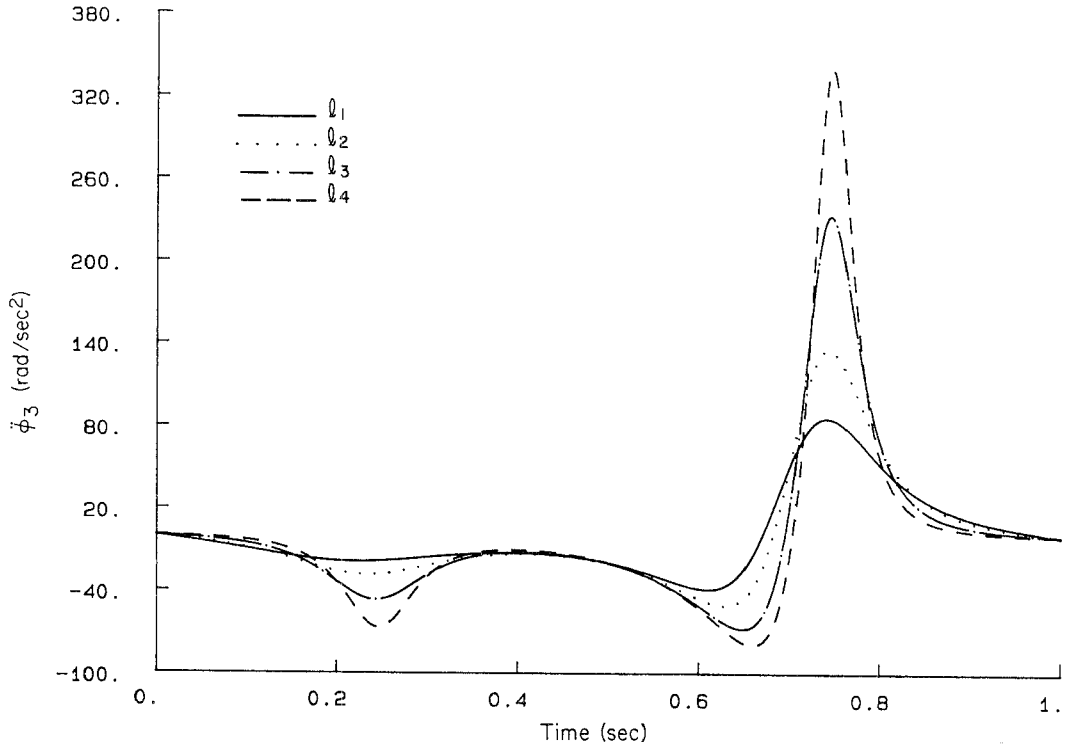

Figure 5.3.8 $\ddot{\phi}$ of follower versus time, model 1.

the curve of Fig. 5.3.6. The extreme behavior of velocity and especially acceleration near $t = 0.75$ s is a clear indication of impending singularity as the length of the follower approaches 2. The results obtained are the same with model 2, as expected.

5.3.5 Lock-up Configuration

If the length of the follower is reduced to $\ell_3 = 1.9$, moving point D upward as in the previous cases, it is shorter than the crank. It is geometrically clear that trouble is in the offing. Plots of $\dot{\phi}_3$ and $\ddot{\phi}_3$ versus time in Fig. 5.3.9 show that lock-up occurs near $t = 0.18$ s, where both approach infinity.

5.4 KINEMATIC ANALYSIS OF A QUICK-RETURN MECHANISM

As an example of the many compound mechanisms that arise in practice (e.g., the shaper of Fig. 1.1.8, the serial manipulator of Fig. 1.1.9, or the vehicle of

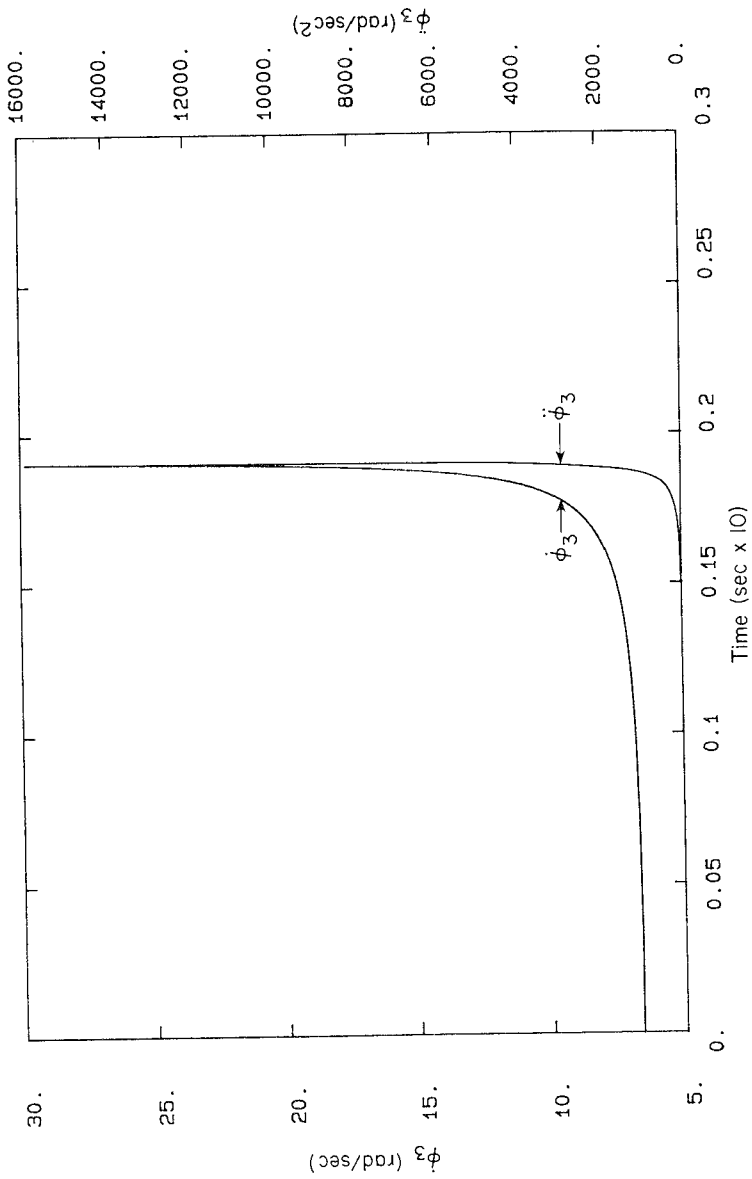

Figure 5.3.9 $\dot{\phi}$ and $\ddot{\phi}$ of follower versus time, lock-up case, model 1.

Figs. 1.1.10, 1.1.11, and 1.1.12), the quick-return mechanism of Fig. 5.4.1 that represents a shaper is considered. With counterclockwise rotation of the crank (body 3), cutting occurs as the tool (body 6) moves to the left through the workpiece (see Fig. 1.1.8). The quick-return stroke of the tool occurs as it moves to the right.

5.4.1 Alternative Models

A quick-return mechanism is modeled here in two different ways. In the model of Fig. 5.4.1, each link is modeled as a body. Elements of the model are as follows:

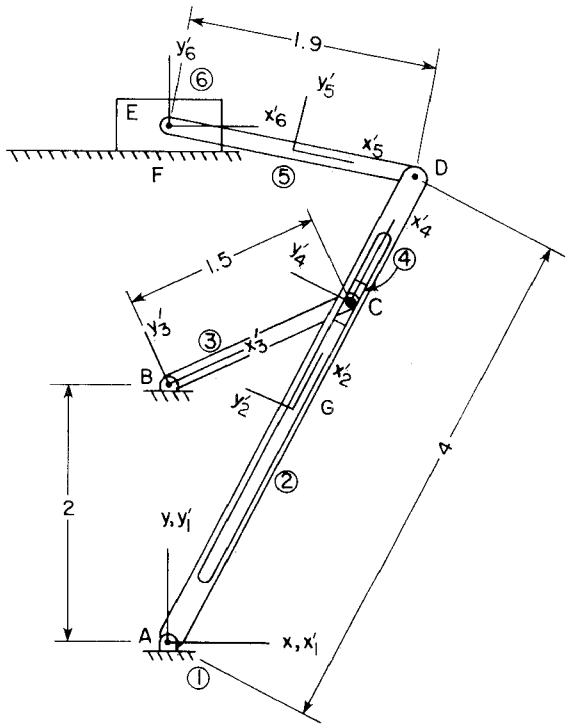

Model 1		
Bodies		
Six bodies		$nc = 18$
Constraints		
Revolute joints:	A	2
	B	2
	C	2
	D	2
	E	2
Translational joints:	C	2
	F	2
Ground constraints (body 1)		3
		$nh = 17$
Thus, DOF = 18 − 17 = 1.		

Figure 5.4.1 Quick-return mechanism, model 1.

Body 1 is ground, and the body-fixed frames of bodies 1 to 6 are shown in Fig. 5.4.1. Revolute joint definition data are given in Table 5.4.1.

Vectors that define the two translational joints are shown in Fig. 5.4.2. Point data that define these vectors, and hence the translational joints, are tabulated in Table 5.4.2.

TABLE 5.4.1 Revolute Joint Data, Model 1

Joint no.	1	2	3	4	5
Common point P	A	B	C	D	E
Body i	1	1	3	2	5
$x_i'^P$	0.0	0.0	1.5	2.0	−0.95
$y_i'^P$	0.0	2.0	0.0	0.0	0.0
Body j	2	3	4	5	6
$x_j'^P$	−2.0	0.0	0.0	0.95	0.0
$y_j'^P$	0.0	0.0	0.0	0.0	0.0

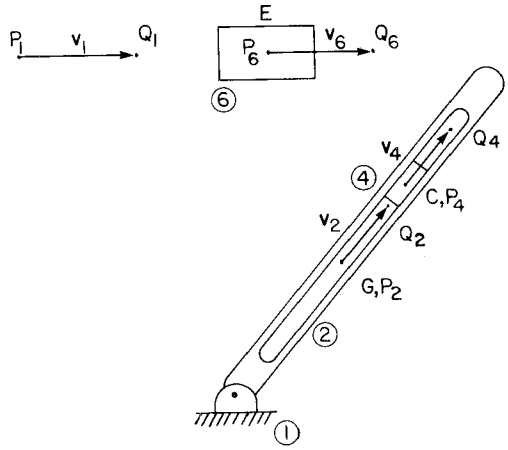

Figure 5.4.2 Translational joint definition, model 1.

TABLE 5.4.2 Translational Joint Data

Vector	$\mathbf{v}_1$	$\mathbf{v}_6$	$\mathbf{v}_2$	$\mathbf{v}_4$
$x_i'^P$	$x_1'^P = -3.0$	$x_6'^P = 0.0$	$x_2'^P = 0.0$	$x_4'^P = 0.0$
$y_i'^P$	$y_1'^P = 4.0$	$y_6'^P = 0.0$	$y_2'^P = 0.0$	$y_4'^P = 0.0$
$x_i'^Q$	$x_1'^Q = -2.0$	$x_6'^Q = 1.0$	$x_2'^Q = 1.0$	$x_4'^Q = 1.0$
$y_i'^Q$	$y_1'^Q = 4.0$	$y_6'^Q = 0.0$	$y_2'^Q = 0.0$	$y_4'^Q = 0.0$

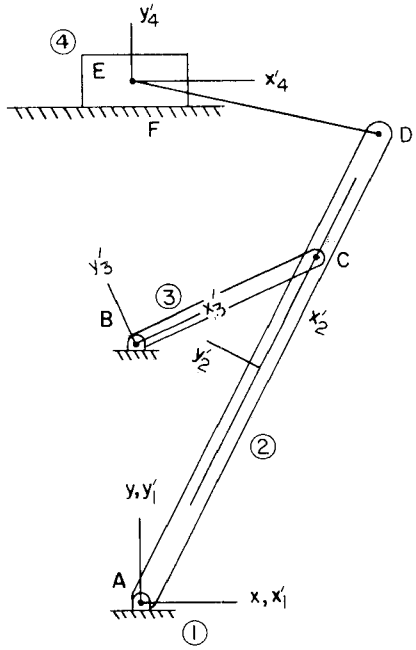

Figure 5.4.3 Quick-return mechanism, model 2.

In model 2 of Fig. 5.4.3, link DE is replaced by a revolute–revolute composite joint, and the slider block at point C is replaced by a revolute–translational joint. The mechanism is thus modeled as follows:

Model 2		
Bodies		
Four bodies		$nc = 12$
Constraints		
Revolute joints:	A	2
	B	2
Translational joint:	F	2
Revolute–revolute joint:	DE	1
Revolute–translational joint:	C	1
Ground constraints (body 1)		3
		$nh = 11$
Thus, DOF = 12 − 11 = 1.		

The same lengths and data used to define the revolute joints at A and B in model 1 are used to define these joints in model 2 (see Table 5.4.1). Similarly, data used to define the translational joint at F in model 1 are used to define the

corresponding joint in model 2 (see Table 5.4.2). The revolute–revolute joint DE is defined in Table 5.4.3, and the revolute–translational joint at C is defined in Table 5.4.4. (see Fig. 5.4.2).

TABLE 5.4.3 Revolute–Revolute Joint *DE*, Model 2

Length of $DE = 1.90$	
Point E (body 4)	Point D (body 2)
$x_4'^E = 0.0$	$x_2'^D = 2.0$
$y_4'^E = 0.0$	$y_2'^D = 0.0$

TABLE 5.4.4 Revolute–Translational Joint at *C*, Model 2

Translational component	Revolute component
(Vector $\mathbf{v}_2$)	
$x_2'^P = 0.0$	$x_3'^P = 1.5$
$y_2'^P = 0.0$	$y_3'^P = 0.0$
$x_2'^Q = 1.0$	
$y_2'^Q = 0.0$	

5.4.2 Assembly

Initial assembly is to be carried out so that the x coordinate of the slider (body 6 in model 1) is zero, that is, with the initial condition $x_6 = 0$. For model 1, initial position and orientation estimates are measured from Fig. 5.4.1, assuming a scale of 1:1. The results of assembly are tabulated in Table 5.4.5.

TABLE 5.4.5 Assembled Configuration, Model 1

Body no.	x	y	ϕ
1	0.0	0.0	0.0
2	0.9190	1.7768	1.0934
3	0.0	2.0	0.4356
4	1.3606	2.6320	1.0938
5	0.9144	3.7766	−0.2368
6	−0.0088	3.9997	0.0

For model 2, position data are obtained from Fig. 5.4.3. The results of assembly are tabulated in Table 5.4.6.

TABLE 5.4.6 Assembled Configuration, Model 2

Body no.	x	y	ϕ
1	0.0	0.0	0.0
2	0.9190	1.7768	1.0934
3	0.0	2.0	0.4356
4	−0.0088	3.9997	0.0

5.4.3 Driver Specification

In both models 1 and 2, there is one kinematic degree of freedom. By placing a driver on ϕ_3, the kinematic model is completed. If body 3 rotates counterclockwise at ω rad/s, the driver takes the form

$$\phi_3 = 0.44 + \omega t$$

5.4.4 Analysis

The quick-return mechanism is first analyzed with two driving angular velocities; $\omega_1 = 2\pi$ rad/s and $\omega_2 = 4\pi$ rad/s. Plots of x, $\dot{x}$, and $\ddot{x}$ for the slider (body 6 in model 1) versus time are given in Figs. 5.4.4, 5.4.5, and 5.4.6, respectively.

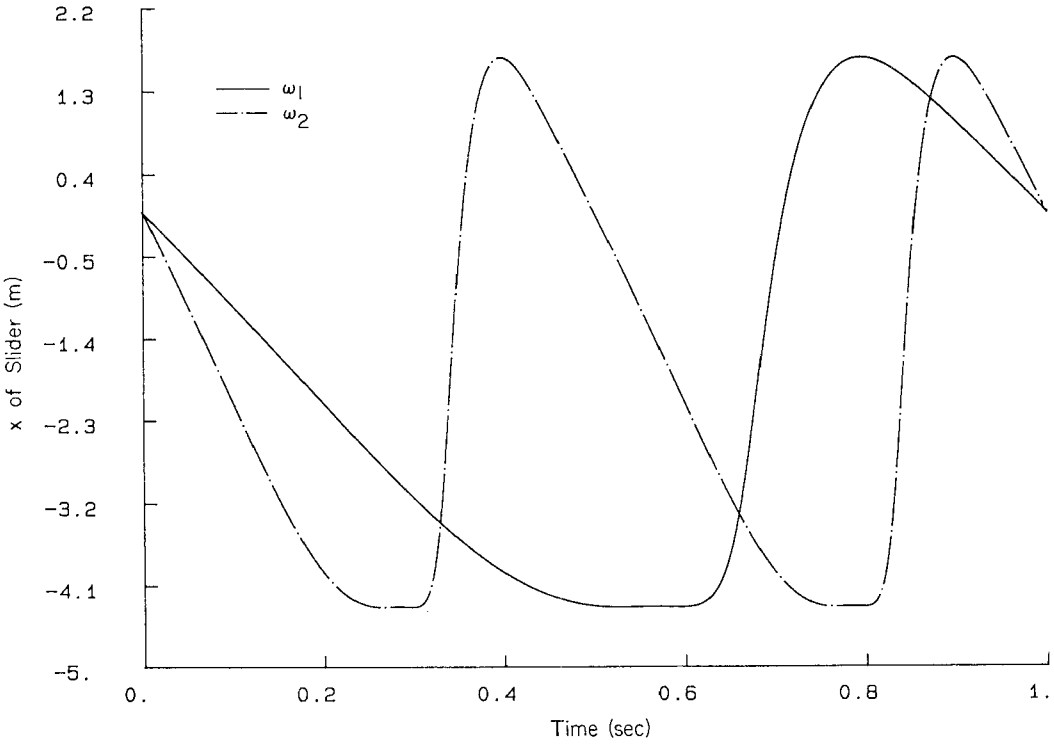

Figure 5.4.4 x of slider versus time.

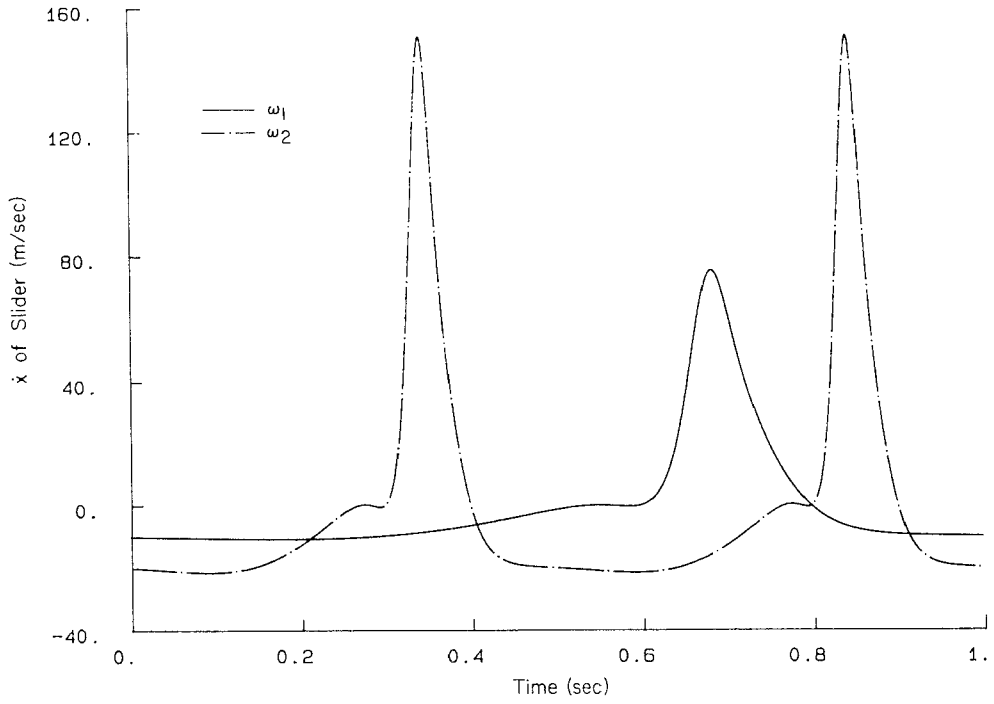

Figure 5.4.5 $\dot{x}$ of slider versus time.

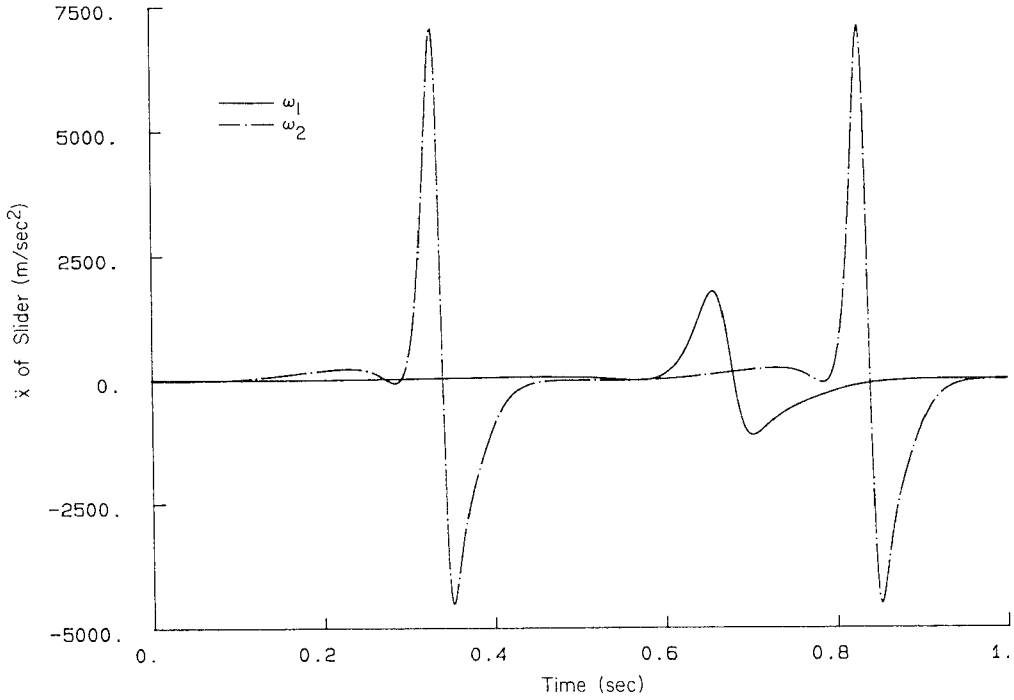

Figure 5.4.6 $\ddot{x}$ of slider versus time.

Identical results are obtained with model 2. Since motion is periodic, the amplitude of motion for both driving speeds is the same. Figures 5.4.5 and 5.4.6, however, show that the ratios of peak velocities and peak accelerations, due to doubling the driving velocity, are approximately 2 and 4, respectively. This behaviour is due to the quadratic dependence of the right side of the acceleration equation on velocity, as noted for the slider–crank analysis of Section 5.2.4.

Note that for ω_1 the leftward stroke of the slider (the cutting tool in a shaper) begins at 0.8 s and continues to about 1.5 s (a repetition of the curve from 0.0 to 0.5 s), with nearly constant velocity (confirmed by the velocity plot of Fig. 5.4.5). This means that 70% of the cycle time of the mechanism is devoted to the cutting stroke and only 30% to the return stroke; hence the name quick-return mechanism. Of further interest, note the nearly constant position of the slider (called *dwell*) during the period 0.5 to 0.6 s. This period would permit an auxiliary mechanism to lift the tool from the workpiece, prior to the return

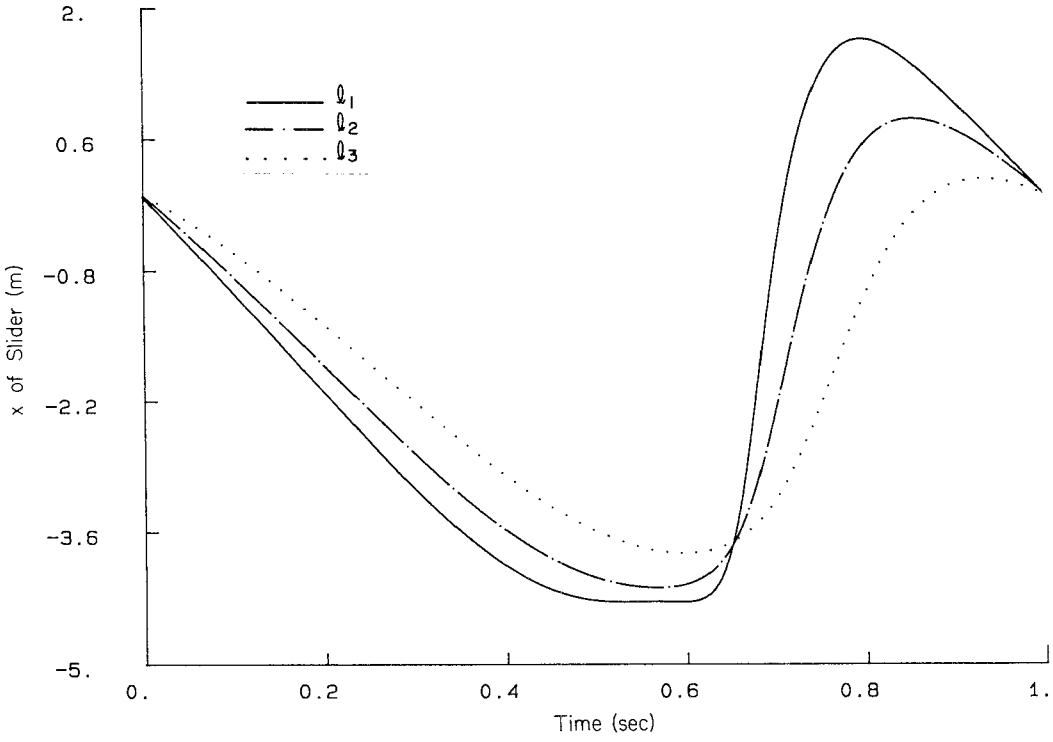

Figure 5.4.7 x of slider versus time with design variations.

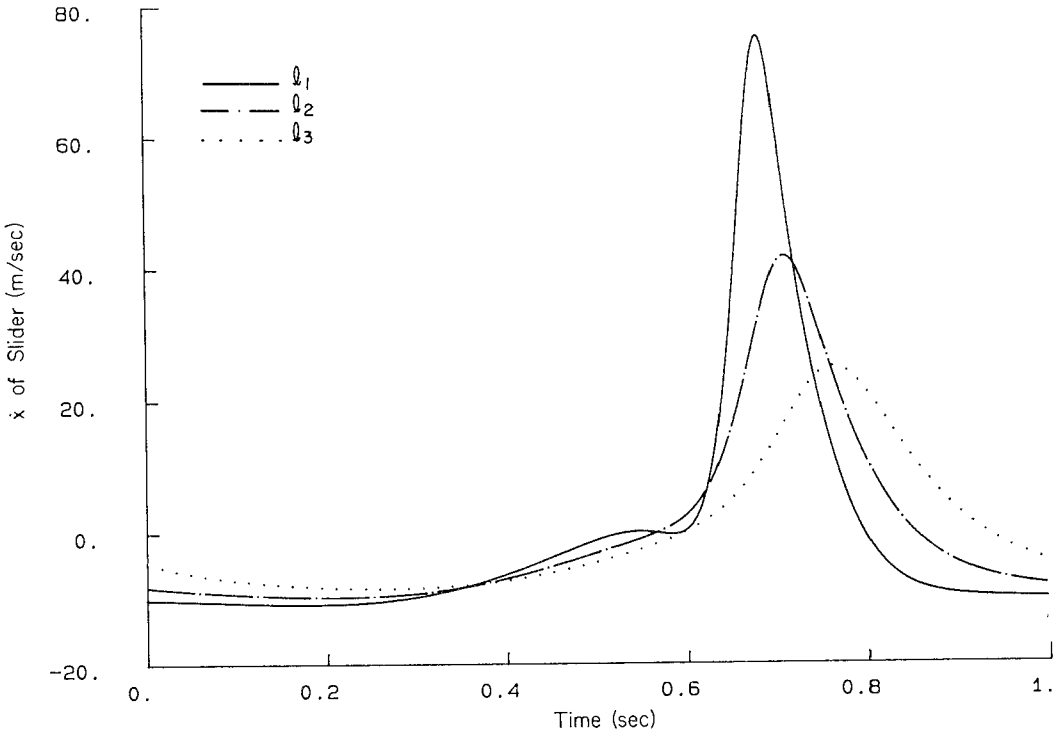

Figure 5.4.8 $\dot{x}$ of slider versus time with design variations.

stroke. It is the essentially nonlinear nature of the kinematic equations that yields these peculiar and often valuable nonlinear characteristics of machines.

As a final consideration, the effect of reducing the length of the crank (body 3 in model 1) is analyzed by carrying out simulations with $\ell_1 = 1.5$ (the previous design), $\ell_2 = 1.25$, and $\ell_3 = 1.0$ For each design, initial assembly is carried out with the slider in the same position to facilitate comparison of performance. The driver is adjusted to rotate the crank at $\omega_1 = 2\pi$ rad/s from the initially assembled configuration. Plots of x, $\dot{x}$, and $\ddot{x}$ for the slider, with each of the designs, are presented in Figs. 5.4.7, 5.4.8, and 5.4.9, respectively.

Note that the reduced crank lengths lead to somewhat reduced stroke lengths, but a comparable fraction of the total stroke is devoted to cutting. They do, however, lead to marked reduction in peak accelerations of the slider, and hence significant reductions in reaction forces in joints. Finally, note that only the nominal design (ℓ_1) exhibits the dwell in position at the left extreme position of the slider.

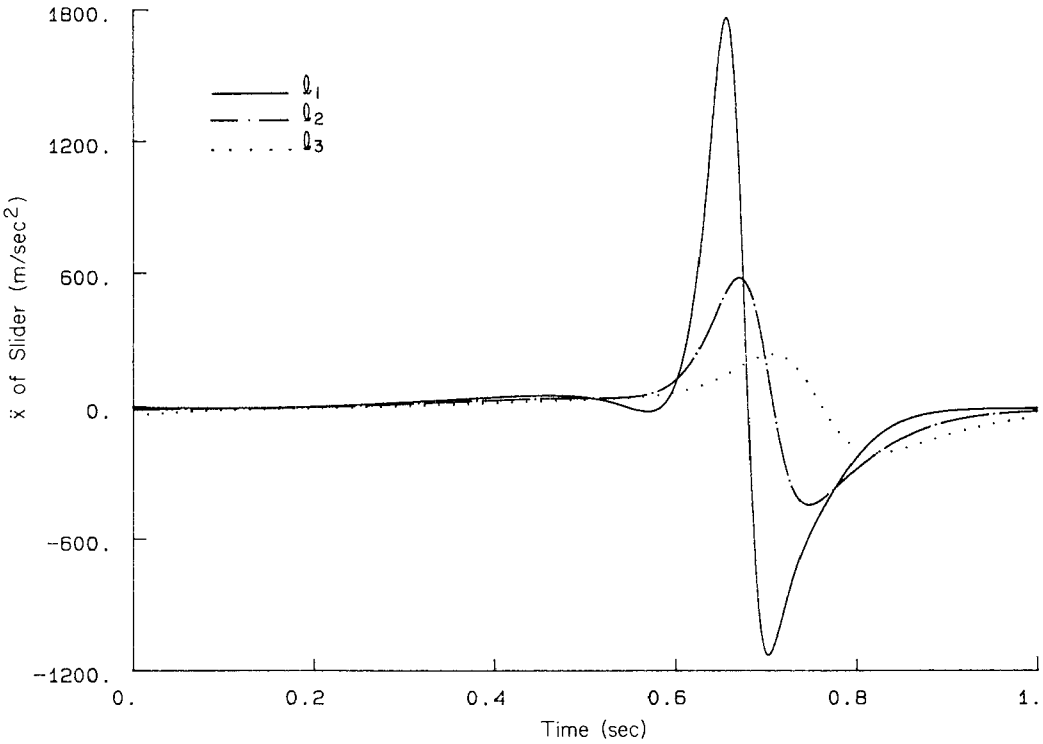

Figure 5.4.9 $\ddot{x}$ of slider versus time with design variations.

5.5 KINEMATIC ANALYSIS OF A GEAR–SLIDER MECHANISM

A compound mechanism that contains a gear set that drives a variable stroke slider mechanism is shown in Fig. 5.5.1. The three-gear arrangement permits input rotation of the first gear (body 2) to be transmitted to the third gear (body 4), even when body 5 is rotated to control the stroke of the slider (body 6).

5.5.1 Kinematic Model

The gear–slider mechanism is modeled as shown in Fig. 5.5.1. This mechanism is composed of six bodies. Bodies 1 to 6 are ground (body 1), three gears (bodies 2, 3, and 4), a stroke control link (body 5), and a slider (body 6).

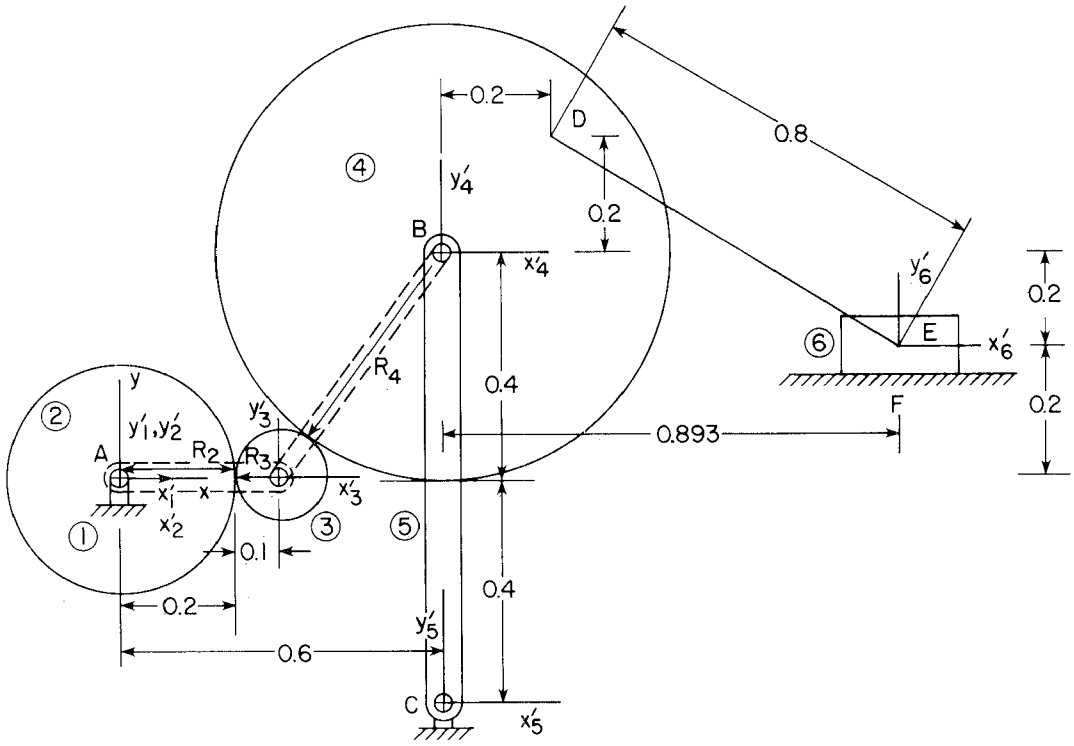

Figure 5.5.1 Gear–slider mechanism.

Kinematic joints between bodies are modeled as follows:

Bodies	
Six bodies	$nc = 18$
Constraints	
Three revolute joints	$3 \times 2 = 6$
Ground–gear 2 (Point A)	
Gear 4–link 5 (Point B)	
Link 5–ground (Point C)	
Two gear set joints	$2 \times 1 = 2$
Gear 2–Gear 3	
Gear 3–Gear 4	
Three distance constraints	$3 \times 1 = 3$
Gear 2–gear 3	
Gear 3–gear 4	
Gear 4–slider	
One translational joint	$2 \times 1 = 2$
Slider–ground (point F)	
One ground constraint (point A)	$3 \times 1 = 3$
	$nh = 16$
Thus, DOF = 18 − 16 = 2	

TABLE 5.5.1 Revolute Joint Data

Joint no.	1	2	3
Common point P	A	B	C
Body i	1	4	5
$x_i'^P$	0.0	0.0	0.0
$y_i'^P$	0.0	0.0	0.0
Body j	2	5	1
$x_j'^P$	0.0	0.0	0.6
$y_j'^P$	0.0	0.8	−0.4

TABLE 5.5.2 Gear Set Data

Joint no.	1	2
Reference points	R_1	R_2
Body i	2	3
Reference angle	0.0	0.9273
Body j	3	4
Reference angle	3.1416	4.0689

TABLE 5.5.3 Distance Constraint Data

Constraint no.	1	2	3
Body i	2	3	4
x_i'	0.0	0.0	0.2
y_i'	0.0	0.0	0.2
Body j	3	4	6
x_j'	0.0	0.0	0.0
y_j'	0.0	0.0	0.0
Distance	0.3	0.5	0.8

TABLE 5.5.4 Translational Joint Data

Body no.	6	1
x'^P	0.0	0.0
y'^P	0.0	0.2
x'^Q	1.0	1.0
y'^Q	0.0	0.2

The radii of gears 2, 3, and 4 are 0.2, 0.1, and 0.4, respectively. The length of link 5 is 0.8. Kinematic joint definition data are summarized in Tables 5.5.1 to 5.5.4.

5.5.2 Assembly

Initial position and orientation estimates are measured from Fig. 5.5.1. The results of assembly calculations are tabulated in Table 5.5.5.

TABLE 5.5.5 Assembled Configuration

Body no.	x	y	ϕ
1	0.0	0.0	0.0
2	0.0	0.0	0.0
3	0.3	0.0	0.0
4	0.6	0.4	0.0
5	0.6	−0.4	0.0
6	1.4928	0.2	0.0

5.5.3 Driver Specification

Two driving constraints are imposed on the gear of body 2 and the stroke control link (body 5). The first driving constraint is a constant angular velocity of the gear of body 2,

$$\phi_2 = 4\pi t$$

The second is a fixed angular position of link 5,

$$\phi_5 = \theta$$

By changing the angle θ of the second driving constraint, the range of slider motion can be varied. Three values of θ are considered: $\theta_1 = -0.1047$, $\theta_2 = 0.0$, and $\theta_3 = 0.5236$ rad. To avoid a lock-up configuration, θ must be in the range $0.7330 < \theta < -0.1204$.

5.5.4 Analysis

Figures 5.5.2 to 5.5.4 are plots of x positions, velocities, and accelerations of the slider for three different values of θ. Note that, even though the stroke of the slider varies significantly with θ, the time histories of velocity and acceleration of the slider do not significantly vary.

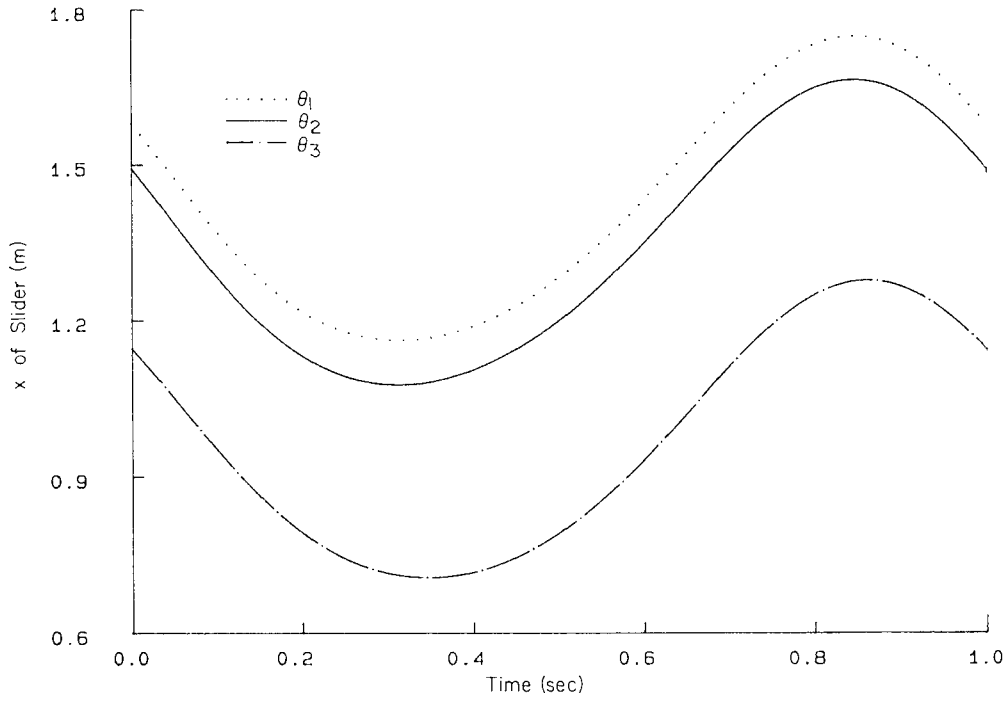

Figure 5.5.2 x of slider versus time.

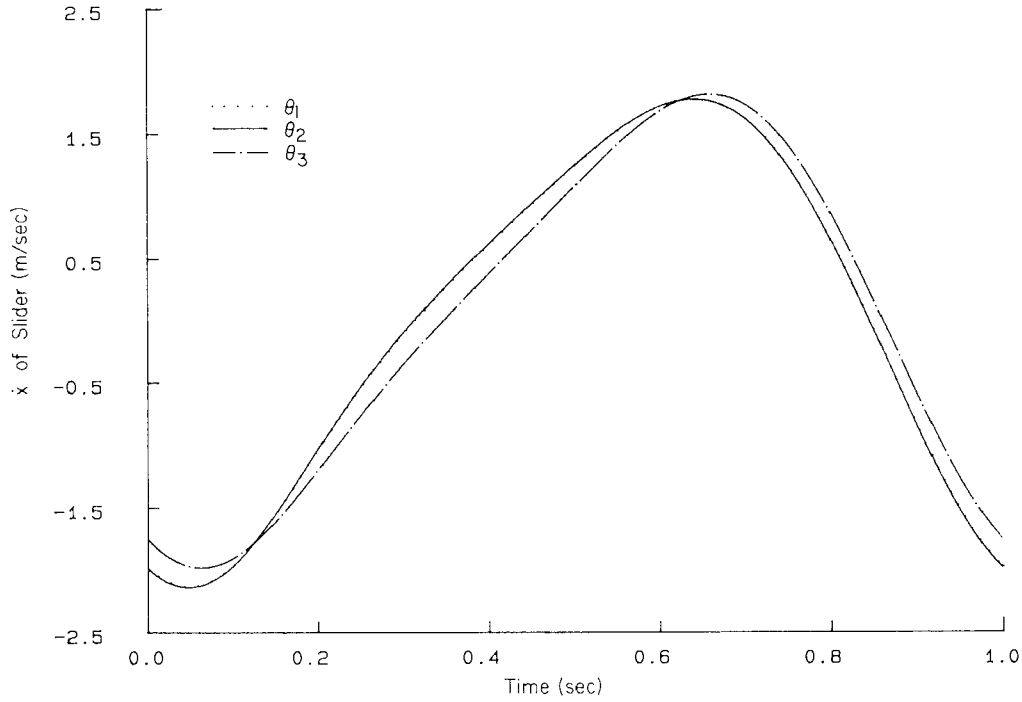

Figure 5.5.3 $\dot{x}$ of slider versus time.

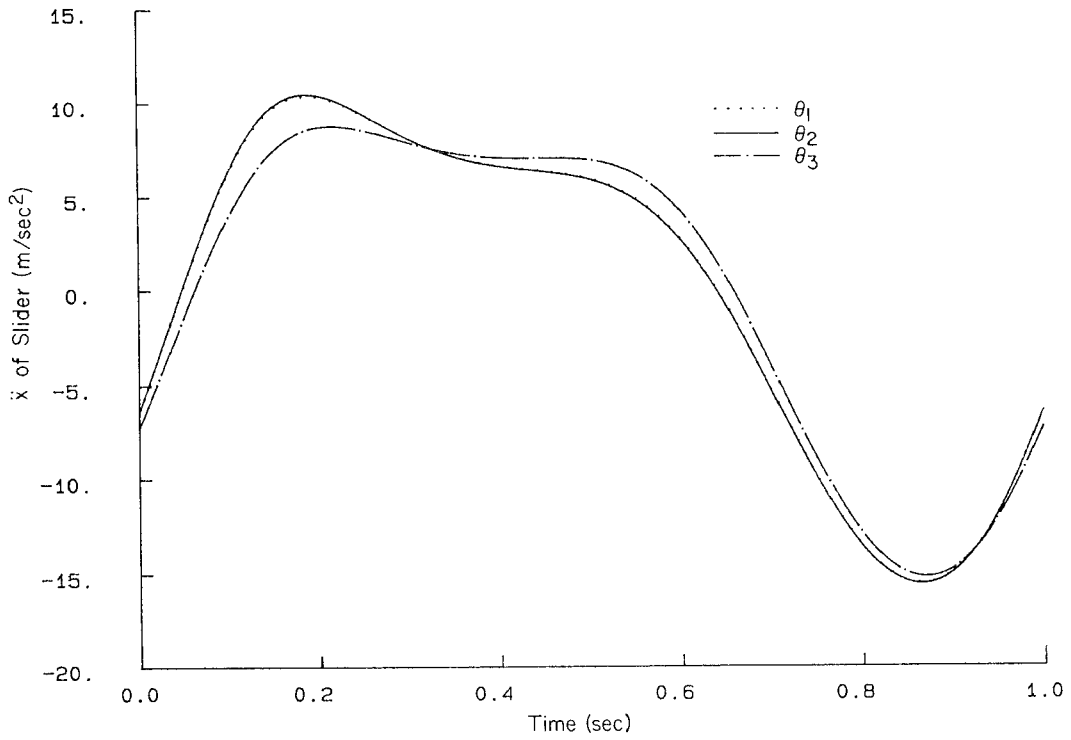

Figure 5.5.4 $\ddot{x}$ of slider versus time.

5.6 KINEMATIC ANALYSIS OF A VALVE-LIFTER MECHANISM

Cam-driven mechanisms are commonly used to create desired time histories of motion, such as in the valve-lifter mechanism of an engine (as in Fig. 1.1.1), shown schematically in Fig. 5.6.1. A cam–flat-faced follower is studied in this section, driving a rocker arm mechanism that controls valve position in an overhead cam engine.

5.6.1 Valve-Lifter Mechanism Model

As an example of a valve-lifter mechanism model, a simple circular cam–flat-faced follower is shown in Fig. 5.6.1, with the cam center offset from the pivot at point B in ground to induce follower motion due to imposed angular motion of the cam. A rocker arm is pivoted with a revolute joint in ground at point C. Revolute–translational composite joints are used to couple the rocker to the follower at point F and the valve stem at point G. The follower and valve stem are constrained to translate relative to ground, as shown in Fig. 5.6.1.

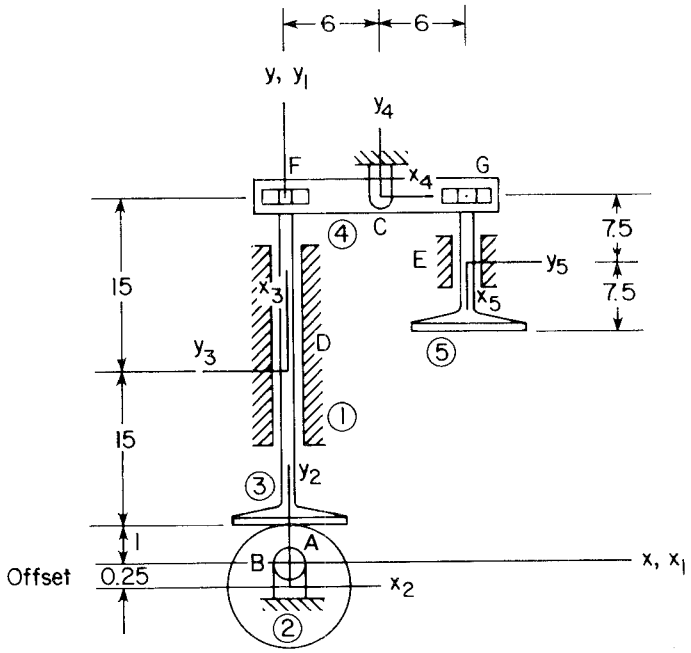

Figure 5.6.1 Valve-lifter mechanism.

Five bodies, including ground, are employed in this model, with constraints defined as follows:

Model		
Bodies		
Five bodies		$nc = 15$
Constraints		
Cam–flat-faced follower joint:	A	1
Revolute joints:	B	2
	C	2
Translational joints:	D	2
	E	2
Revolute–translational joints:	F	1
	G	1
Ground constraints		3
		$nh = 14$
Thus, DOF = 15 − 14 = 1.		

To prescribe motion, the one remaining degree of freedom is eliminated by specifying the angular velocity of the cam shaft; that is, by placing an angle driver on ϕ_2.

TABLE 5.6.1 Cam–Flat-faced Follower Joint Data

Shape center Q of body 2 (cam)	
$x_2'^Q$	0
$y_2'^Q$	0
Shape perfect circle with radius	1.25
Revolute joint offset	0.25
P on body 3 (follower): $x_3'^P$	−15
$y_3'^P$	0
Q on body 3 (follower): $x_3'^Q$	−15
$y_3'^Q$	1

As an elementary numerical example, a circular cam of radius 1.25 cm (all data in this example are given in centimeters) is employed. Data defining the cam–flat-faced follower between bodies 2 and 3 are given in Table 5.6.1.

Revolute joints between the cam and ground at point B and between the rocker and ground at point C are imposed, with data specified in Table 5.6.2. Translational joints between the follower and valve stem and ground are specified by data given in Table 5.6.3. Vector $\mathbf{v}_{11}$ is in ground, located between point D and a point one unit above D. Vector $\mathbf{v}_3$ is fixed in the follower between the point at the origin of the x_3-y_3 frame and a point one unit above. Similarly, vectors $\mathbf{v}_{12}$ in ground and $\mathbf{v}_5$ in the valve stem define the translational joint at point E.

Finally, revolute–translational joints between the follower and valve stem and the rocker at points F and G are specified by the vectors shown in Fig. 5.6.2

TABLE 5.6.2 Revolute Joint Data

Joint no.	1	2
Common point P	B	C
Body i	1	4
$x_i'^P$	0.0	0.0
$y_i'^P$	0.0	0.0
Body j	2	1
$x_j'^P$	0.0	6.0
$y_j'^P$	0.25	31.0

TABLE 5.6.3 Translational Joint Data

Vector	$\mathbf{v}_{11}$	$\mathbf{v}_3$	$\mathbf{v}_{12}$	$\mathbf{v}_5$
$x_i'^P$	$x_{11}'^P = 0.0$	$x_3'^P = 0.0$	$x_{12}'^P = 12.0$	$x_5'^P = 0.0$
$y_i'^P$	$y_{11}'^P = 16.0$	$y_3'^P = 0.0$	$y_{12}'^P = 23.5$	$y_5'^P = 0.0$
$x_i'^Q$	$x_{11}'^Q = 0.0$	$x_3'^Q = 1.0$	$x_{12}'^Q = 12.0$	$x_5'^Q = 1.0$
$y_i'^Q$	$y_{11}'^Q = 17.0$	$y_3'^Q = 0.0$	$y_{12}'^Q = 22.5$	$y_5'^Q = 0.0$

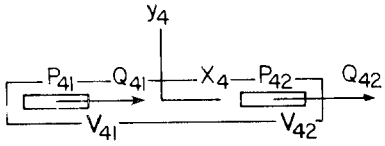

Figure 5.6.2 Revolute–translational joints.

on the rocker. Data that define the locations of points P and Q, and hence the vectors $\mathbf{v}_{41}$ and $\mathbf{v}_{42}$, are given in Table 5.6.4. The locations of revolute joints of the couplers in the follower and valve stem, bodies 3 and 5, respectively, are also prescribed in Table 5.6.4.

TABLE 5.6.4 Revolute–Translational Joint Data

Translational components		
Vector	$\mathbf{v}_{41}$	$\mathbf{v}_{42}$
$x_i'^P$	$x_{41}'^P = -6.0$	$x_{42}'^P = 6.0$
$y_i'^P$	$y_{41}'^P = 0.0$	$y_{42}'^P = 0.0$
$x_i'^Q$	$x_{41}'^Q = -5.0$	$x_{42}'^Q = 7.0$
$y_i'^Q$	$y_{41}'^Q = 0.0$	$y_{42}'^Q = 0.0$
Revolute components		
Body 3	Body 5	
$x_3'^P = 15.0$	$x_5'^P = -7.5$	
$y_3'^P = 0.0$	$y_3'^P = 0.0$	

5.6.2 Assembly

The configuration of the valve-lifter mechanism shown in Fig. 5.6.1 permits easy generation of accurate initial estimates for the location and orientation of bodies. The results of numerical assembly analysis, holding $\phi_2 = 0$, are presented in Table 5.6.5.

TABLE 5.6.5 Assembled Configuration

Body no.	x	y	ϕ
1	0.0	0.0	0.0
2	0.0	−0.2500	0.0
3	0.0	16.0000	1.5708
4	6.0000	31.0000	0.0
5	12.0000	23.5000	4.7124

5.6.3 Driver Specification

The mechanism is driven by specifying a cam angular velocity of 20 revolutions per second; that is, with the driver

$$\phi_2 = 40\pi t$$

5.6.4 Analysis

To investigate the effect of variations in cam geometry on motion of the valve lifter, the eccentricity of the circular cam used in this study is varied from the nominal value $e_1 = 0.25$ cm shown in Fig. 5.6.1 to $e_2 = 0.35$ cm and $e_3 = 0.45$ cm. To maintain the geometry shown in Fig. 5.6.1, the height of the revolute joint at point B between the cam (body 2) and ground is set equal to the eccentricity in each case, leaving the initial height of the follower at point A unchanged for each design.

Valve stem position, velocity, and acceleration versus time, for each of the three cam eccentricities, are plotted in Figs. 5.6.3 to 5.6.5, respectively. As expected on physical grounds, the cyclic behavior of each of the three designs is

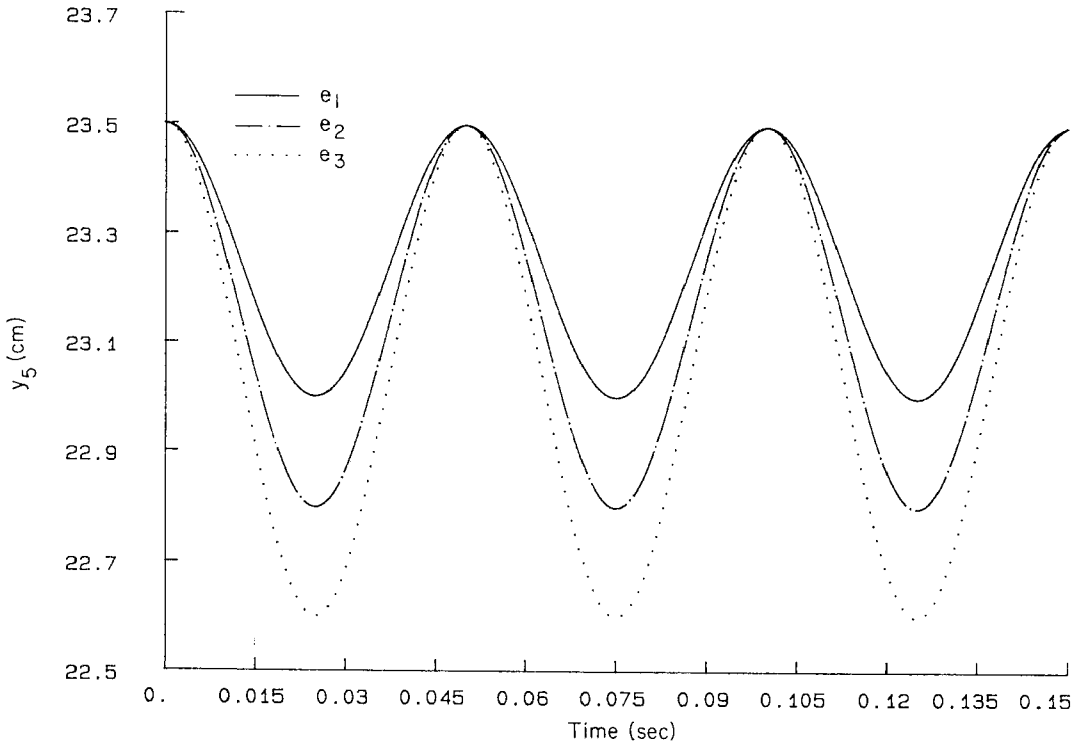

Figure 5.6.3 Valve stem position versus time.

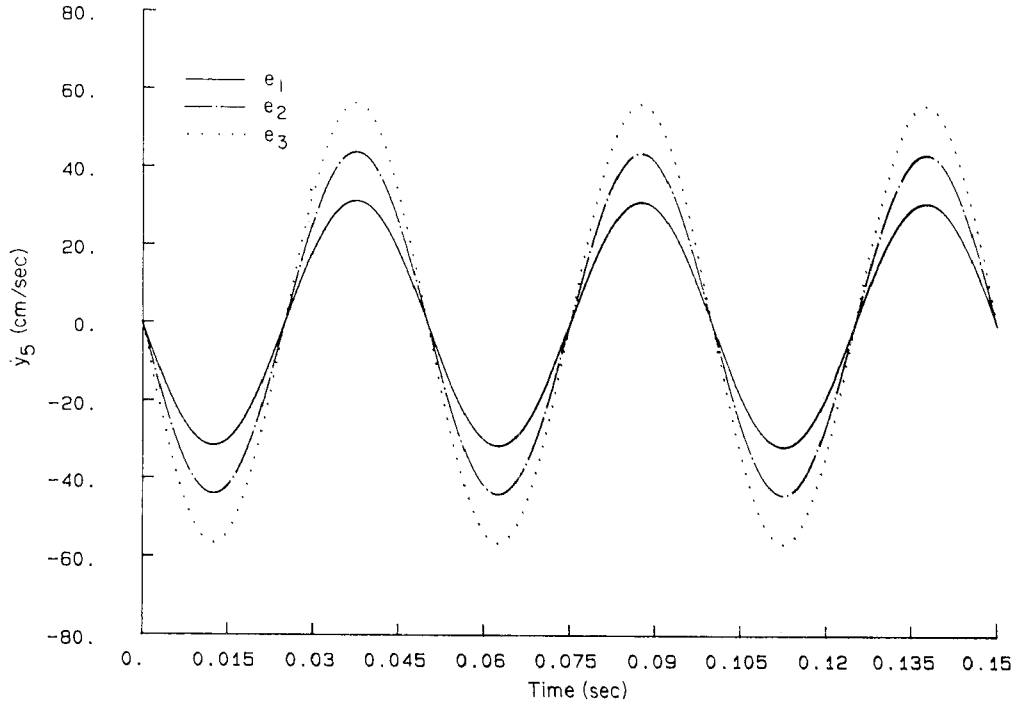

Figure 5.6.4 Valve stem velocity versus time.

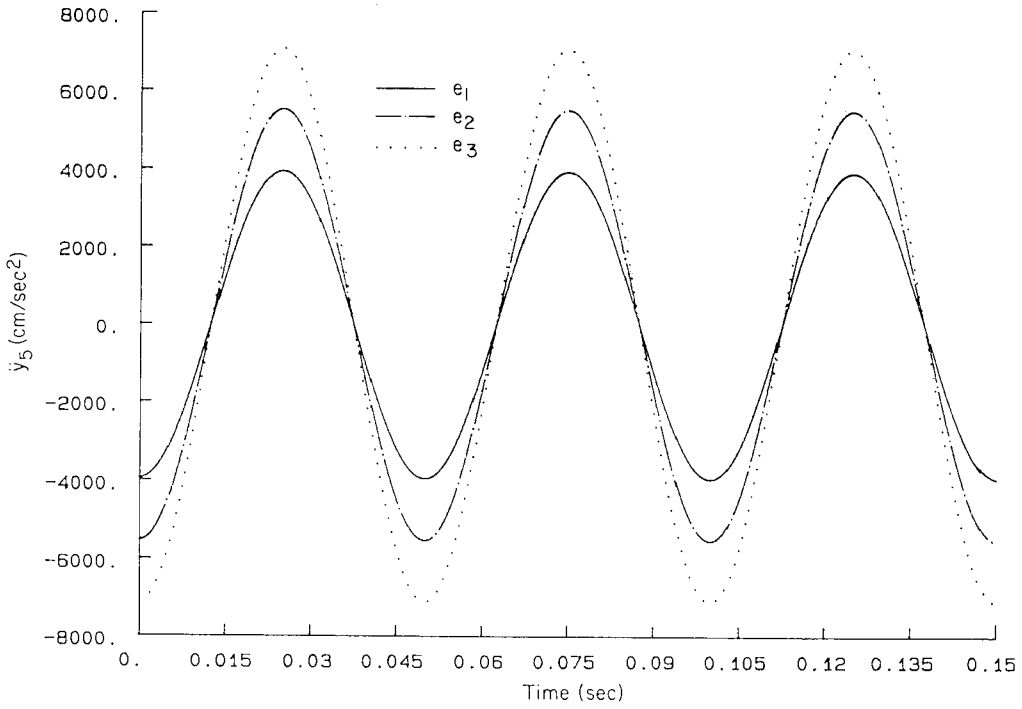

Figure 5.6.5 Valve stem acceleration versus time.

very similar, with only amplitude varying. The essentially sinusoidal character of the response of the valve lifter in this elementary example is associated with the circular cam. In automotive applications, an essentially circular cam surface, with center at the pivot point B, is employed, with a distinct lobe that causes valve motion. As a result, a shorter and more distinct response of the valve stem occurs, with a dwell in the closed position for most of the rotation of the cam.

DADS PROJECTS

5.1. Consider the film follower mechanism shown in Fig. P5.1. The mechanism can be modeled using four bodies: ground, a crank, a rocker arm, and a follower. A point of interest P is defined on the end of the follower. It is this point that engages and disengages the film as the mechanism moves. The crank rotates counterclockwise at 1000 rpm. Construct a DADS model for kinematic analysis, using the following procedures:

(a) Count the number of generalized coordinates and constraints to find the number of DOF and check physically.

(b) Draw each body separately and define body-fixed frames, joint definition points, and point of interest.

(c) Create DADS input data and run.

(d) Plot

(i) y^P of the point of interest versus x^P of the point of interest.

(ii) $\dot{x}^P$ of the point of interest versus time.

(iii) $\ddot{x}^P$ of the point of interest versus time.

(iv) $\dot{y}^P$ of the point of interest versus time.

(v) $\ddot{y}^P$ of the point of interest versus time.

(e) Give a physical interpretation of the plots obtained and discuss kinematic singularities, if any exist.

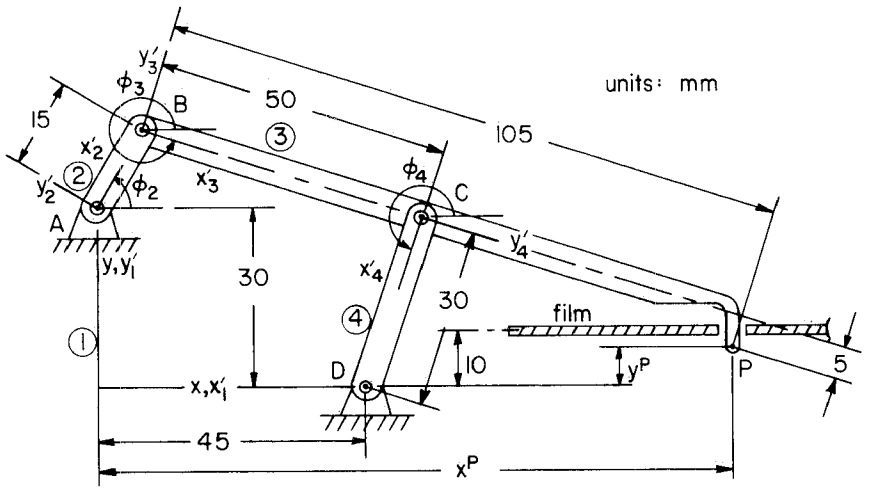

Figure P5.1

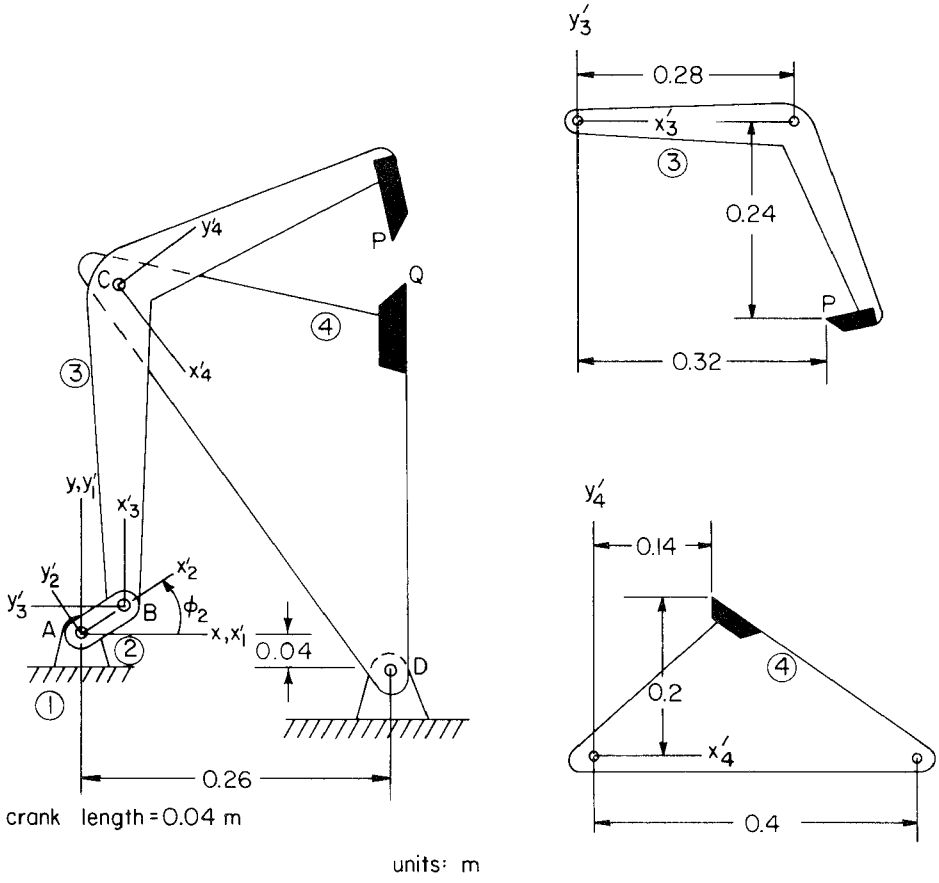

Figure P5.2

5.2. Consider the web cutting mechanism shown in Fig. P5.2. The model has four bodies: ground, a crank, a knife-arm, and a rocker arm. Points of interest P and Q are defined on the tips of the cutting blades. The x velocities of these points are of particular interest. In an actual mechanism, a sheet of fabric or metal is fed between the blades and the blade tips come together periodically to slice off a section of the web. The machine is designed such that the x velocity of the blade tips matches very closely the velocity of the web. This allows for a clean cut, with little or no tearing. The crank is driven with an angular velocity of 60 rpm. Construct a DADS model for kinematic analysis, following steps (a) through (c) of DADS Project 5.1, and

(d) Draw two curves on one plot for:

- **(i)** x^P and x^Q versus time.
- **(ii)** $\dot{x}^P$ and $\dot{x}^Q$ versus time.
- **(iii)** $\ddot{x}^P$ and $\ddot{x}^Q$ versus time.
- **(iv)** y^P and y^Q versus time.
- **(v)** $\dot{y}^P$ and $\dot{y}^Q$ versus time.

(vi) $\ddot{y}^P$ and $\ddot{y}^Q$ versus time.

(e) Monitor how close the x positions of points P and Q agree throughout the simulation. If there is a time interval over which x^P and x^Q differ, discuss this position difference concerning y^P and y^Q. Suggest any design changes that may be necessary.

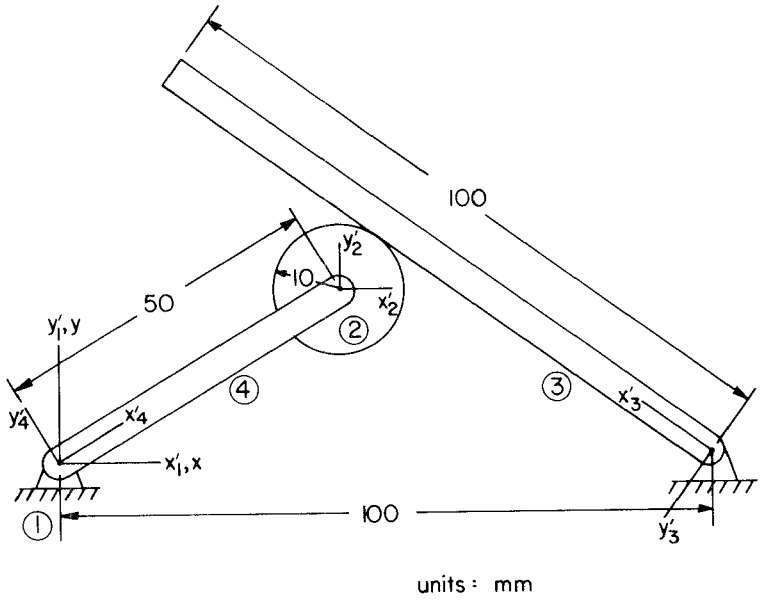

Figure P5.3

5.3. Consider the mechanism shown in Fig. P5.3, which uses a rack and pinion joint. The four bodies used are ground, the rack, the pinion, and the coupler. The pinion rotates clockwise at 60 rpm. Construct a DADS model for kinematic analysis, following steps (a) to (c) of DADS Project 5.1, and

(d) Plot:

(i) x, $\dot{x}$, and $\ddot{x}$ of the pinion versus time.

(ii) y, $\dot{y}$, and $\ddot{y}$ of the pinion versus time.

(iii) ϕ, $\dot{\phi}$, and $\ddot{\phi}$ of the rack versus time.

(e) Create an alternative three-body model by replacing the coupler with a revolute–revolute joint. Compare results with those of the four-body model.